Atmos. Chem. Phys., 24, 4789–4807, 2024
https://doi.org/10.5194/acp-24-4789-2024
© Author(s) 2024. This work is distributed under
the Creative Commons Attribution 4.0 License.

Atmospheric Chemistry and Physics
Open Access
EGU

Impact of HO_2/RO_2 ratio on highly oxygenated α-pinene photooxidation products and secondary organic aerosol formation potential

Yarê Baker[1], Sungah Kang[1], Hui Wang[1], Rongrong Wu[1], Jian Xu[1], Annika Zanders[1], Quanfu He[1], Thorsten Hohaus[1], Till Ziehm[1], Veronica Geretti[2], Thomas J. Bannan[3], Simon P. O'Meara[3,4], Aristeidis Voliotis[3], Mattias Hallquist[2], Gordon McFiggans[3], Sören R. Zorn[1], Andreas Wahner[1], and Thomas F. Mentel[1]

[1]Institute for Energy and Climate Research, IEK-8, Forschungszentrum Jülich, 52425 Jülich, Germany
[2]Atmospheric Science, Department of Chemistry and Molecular Biology, University of Gothenburg, 41296 Gothenburg, Sweden
[3]Department for Earth and Environmental Sciences, University of Manchester, Manchester M13 9PL, UK
[4]National Centre for Atmospheric Science, University of Manchester, Manchester M13 9PL, UK

Correspondence: Thomas F. Mentel (t.mentel@fz-juelich.de)

Received: 21 October 2023 – Discussion started: 26 October 2023
Revised: 31 January 2024 – Accepted: 8 February 2024 – Published: 22 April 2024

Abstract. Highly oxygenated molecules (HOMs) from the atmospheric oxidation of biogenic volatile organic compounds are important contributors to secondary organic aerosol (SOA). Organic peroxy radicals (RO_2) and hydroperoxy radicals (HO_2) are key species influencing the HOM product distribution. In laboratory studies, experimental requirements often result in overemphasis on RO_2 cross-reactions compared to reactions of RO_2 with HO_2. We analyzed the photochemical formation of HOMs from α-pinene and their potential to contribute to SOA formation under high ($\approx$ 1/1) and low ($\approx$ 1/100) HO_2/RO_2 conditions. As $HO_2/RO_2 > 1$ is prevalent in the daytime atmosphere, sufficiently high HO_2/RO_2 is crucial to mimic atmospheric conditions and to prevent biases by low HO_2/RO_2 on the HOM product distribution and thus SOA yield. Experiments were performed under steady-state conditions in the new, continuously stirred tank reactor SAPHIR-STAR at Forschungszentrum Jülich. The HO_2/RO_2 ratio was increased by adding CO while keeping the OH concentration constant. We determined the HOM's SOA formation potential, considering its fraction remaining in the gas phase after seeding with $(NH_4)_2SO_4$ aerosol. An increase in HO_2/RO_2 led to a reduction in SOA formation potential, with the main driver being a $\sim$ 60 % reduction in HOM-accretion products. We also observed a shift in HOM-monomer functionalization from carbonyl to hydroperoxide groups. We determined a reduction of the HOM's SOA formation potential by $\sim$ 30 % at $HO_2/RO_2 \approx$ 1/1 compared to $HO_2/RO_2 \approx$ 1/100. Particle-phase observations measured a similar decrease in SOA mass and yield. Our study shows that too low HO_2/RO_2 ratios compared to the atmosphere can lead to an overestimation of SOA yields.

Published by Copernicus Publications on behalf of the European Geosciences Union.

Dedication. Dedicated to Astrid Kiendler-Scharr, deceased 6 February 2023.

1 Introduction

In the atmosphere, highly oxidized products from the oxidation of biogenic or anthropogenic volatile organic compounds (VOCs) are an important source of secondary organic aerosol (SOA) (Roldin et al., 2019; Mohr et al., 2019). SOA is an important contributor to the overall ambient aerosol and of interest because of its impact on climate, visibility and human health (Hallquist et al., 2009).

Recently, many studies (Pullinen et al., 2020; Berndt et al., 2016; Bianchi et al., 2017) have focused on understanding the oxidation pathways of VOCs that yield highly oxygenated molecules (HOMs), as these are expected to be of low enough volatility to condense into the particle phase. One important tool for the investigation of VOC degradation and SOA formation is the utilization of experiments in atmospheric simulation chambers (Hidy, 2019). Such experiments have also helped to elucidate key processes in the HOM formation, i.e., the process of autoxidation.

After an initial oxidant attack and the formation of a peroxy radical (RO_2), autoxidation adds oxygen to the molecule via an internal H shift to the peroxy group, forming a hydroxy peroxide group and an alkyl radical, to which O_2 immediately adds, re-establishing the peroxy functionality. This process can be repeated multiple times, yielding almost instantaneously highly oxygenated peroxy radicals (HOM-RO_2) which are terminated to a series of HOM closed-shell products (Bianchi et al., 2019; Ehn et al., 2014; Crounse et al., 2013).

Chamber studies often work with a singular compound and operate at higher precursor concentrations than those observed in the atmosphere for experimental reasons. These experiments cannot represent the complex mixture of VOCs and oxidized VOCs present in the atmosphere (McFiggans et al., 2019). Higher precursor concentrations can lead, per se, to higher SOA yields than observed in the atmosphere (a well-characterized phenomenon; see Henry et al., 2012, and Shilling et al., 2009) and to a general preference for higher-order processes which may not be important in the atmosphere. One example is that chamber studies tend to overestimate the role of cross-reactions between organic peroxy radicals (RO_2), owing to high precursor concentrations of a single VOC. In chambers, reactions of HOM-RO_2 with other organic peroxy radicals terminate the autoxidation chain, leading typically to multifunctional carbonyl and alcohol compounds. In comparison, in the atmosphere termination by HO_2 is more likely, leading to multifunctional hydroperoxides. In the presence of sufficient NO, termination to multifunctional organic nitrates may be more important (Schervish and Donahue, 2021).

Another possible termination reaction of HOM-RO_2 with HOM-RO_2 and less oxidized RO_2 leads to the formation of accretion products, which are expected to be extremely low volatility organic compounds (ELVOCs) and are therefore expected to contribute to new particle formation and SOA formation (Ehn et al., 2014; Berndt et al., 2018). Schervish and Donahue (2021) raised awareness that chamber studies could overestimate the SOA formation potential from the oxidation of terpenes such as α-pinene compared to the atmosphere because of missing HO_2 and low-molecular-weight RO_2 (e.g., CH_3O_2), which favors accretion product formation. Previous studies of VOC ozonolysis with different OH scavengers by Docherty and Ziemann (2003) and Keywood et al. (2004) indicated a significant impact of the HO_2/RO_2 ratio on SOA yields.

In chamber studies, the use of higher VOC concentrations is often an unavoidable necessity either to match the sensitivity of the analytical instrumentation or to overcome chamber-related effects. The question remains, how can conditions dictated by the chamber be steered towards more realistic chemical pathways and higher atmospheric relevance?

In this study, we address this overestimated importance of peroxy radical cross-reactions. We studied the photooxidation of α-pinene in a series of steady-state experiments in the newly built, continuously stirred tank reactor SAPHIR-STAR (a modernized version of JPAC; see Mentel et al., 2009).

We compared two experimental conditions, a pure α-pinene photooxidation case, leading to low HO_2/RO_2 ratios and high importance of RO_2 cross-reactions, and a high HO_2/RO_2 case, representing more atmospherically relevant conditions with high importance of $RO_2 + HO_2$ reactions. One important concept of the conducted experiments is the constant OH availability to α-pinene in order to prevent effects of different oxidant levels and allow for a direct comparison between the two chemical regimes. To this end, the OH concentration in the experiments was adjusted to keep the α-pinene OH turnover constant and to avoid changes due to oxidant scavenging.

Furthermore, the addition of seed particles ($(NH_4)_2SO_4$) allowed us to observe the condensation behavior of the HOM products and to compare our gas-phase observations directly with particulate-phase measurements of the condensed organic mass.

In this study, we will address two central questions. How does the shift in HO_2/RO_2 impact the oxidation mechanism of α-pinene, especially the HOM formation pathway? And what is the subsequent impact on the SOA formation potential of the α-pinene photooxidation system? As the central analysis tool, we will use high-resolution time-of-flight mass spectrometry with chemical ionization (HR-TOF-CIMS) with nitrate (NO_3^-) reagent ions as this ionization scheme is selective towards HOM compounds (Hyttinen et al., 2018).

2 Methods

2.1 Generic α-pinene HOM peroxy radical chemistry

The chemical mechanistic information for the basic oxidation scheme of α-pinene was taken from the Master Chemical Mechanism (MCM) v3.3.1 (Jenkin et al., 1997; Saunders et al., 2003) (http://mcm.york.ac.uk, last access: 20 October 2023). The main peroxy radicals expected from α-pinene photooxidation are $C_{10}H_{17}O_x$ and $C_{10}H_{15}O_x$. $C_{10}H_{17}O_x$ is formed by the addition of OH to α-pinene, followed by O_2 (starting RO_2: $C_{10}H_{17}O_3$) (MCM v3.3.1 (Jenkin et al., 1997; Saunders et al., 2003)). Studies showed that the autoxidation can start from $C_{10}H_{17}O_3$ with the four-member ring in α-pinene opened (Berndt, 2021; Xu et al., 2019).

For $C_{10}H_{15}O_x$, the autoxidation chain is assumed to start with $C_{10}H_{15}O_4$, which can be formed directly from ozonolysis via the vinyl hydroperoxide path (Johnson and Marston, 2008; Iyer et al., 2021) or via H abstraction from first-generation oxidation products such as pinonaldehyde ($C_{10}H_{16}O_2$) (MCM v3.3.1; Jenkin et al., 1997; Saunders et al., 2003; Fantechi et al., 2002). A recent study suggests direct H abstraction by OH from α-pinene (Shen et al., 2022) as a starting point for the autoxidation chain.

The autoxidation process is rapid with H-shift rates of about 0.01–0.1 s^{-1} and faster (Piletic and Kleindienst, 2022; Berndt, 2021; Xu et al., 2019; Vereecken et al., 2007). The autoxidation chain will run quickly, adding more oxygen to the molecule, until bimolecular termination reactions are able to compete with all available H-shift rates. The rate of an H shift is determined by the hydrogen's position in relation to the peroxy radical and the functional groups near the hydrogen and peroxy radical (Otkjaer et al., 2018; Vereecken and Nozière, 2020). In the absence of NO_x, the peroxy radicals have two major bimolecular termination channels: the reaction with another RO_2 or with HO_2. A third pathway is the intramolecular termination (Rissanen et al., 2014).

Based on the considerations above, we apply a simplified generic reaction scheme to analyze our observations. Figure 1 shows an overview of the reaction pathways for the main peroxy radical families in the α-pinene photooxidation and the resulting product groups and families. The compounds can be separated into four classes; peroxy radicals (HOM-RO_2), monomers (HOM-Mon), accretion products (HOM-Acc) and fragments (HOM-Frag). The HOM-RO_2 class consists of all detected HOM-RO_2, with special focus on the analysis of the C_{10} HOM-RO_2 families. The HOM-Mon class contains the closed-shell HOM-C_{10} products. The compounds in the fragment class contain less than 10 carbon atoms, while all HOM-Acc compounds contain more than 10 carbon atoms. The compound classes are further divided into groups and families. Here, the term group is used for compounds with the same carbon number, while a family contains all compounds with the same carbon and hydrogen number but a varying oxygen number.

The termination of RO_2 with HO_2 will lead to hydroperoxide formation:

$$RO_2 + HO_2 \rightarrow ROOH + O_2. \quad \text{(R1)}$$

In the case of $C_{10}H_{15}O_x$, Reaction (R1) will lead to multifunctional $C_{10}H_{16}O_z$ hydroperoxides (wherein the notation "hydroperoxides", "carbonyls", or "alcohols", etc., here and in the following relates to the functionality of the group formed by the termination reaction). For $C_{10}H_{17}O_x$, it will lead to the formation of $C_{10}H_{18}O_z$ hydroperoxides. The termination via RO_2+RO_2 can either result in the formation of accretion products or in the formation of carbonyls and alcohols. For the accretion product formation, it is assumed that the two RO_2 chemically bond, eliminating O_2 from the molecule:

$$RO_2 + R'O_2 \rightarrow R{-}O{-}O{-}R' + O_2. \quad \text{(R2)}$$

Recombination reactions of the main peroxy radical families $C_{10}H_{15}O_x$ and $C_{10}H_{17}O_x$ lead to the product families $C_{20}H_{30}O_z$ (combination of two $C_{10}H_{15}O_x$), $C_{20}H_{32}O_z$ (combination of $C_{10}H_{15}O_x$ and $C_{10}H_{17}O_x$), and $C_{20}H_{34}O_z$ (combination of two $C_{10}H_{17}O_x$).

However, due to reactions with smaller peroxy radicals, HOM-Acc families with smaller carbon and hydrogen numbers are also observed. Indeed, one reason why the RO_2+$R'O_2$ termination is expected to affect the SOA formation potential is the formation of accretion products by scavenging of less oxidized and low-molecular-weight RO_2 by HOM-RO_2. Thus, the smaller RO_2 will also contribute to the SOA mass which would otherwise not be the case. For the HOM-RO_2 itself, it is expected that they contribute to SOA formation independently of the termination pathway, due to the low volatility of its expected termination products (Pullinen et al., 2020; McFiggans et al., 2019).

The second RO_2+$R'O_2$ termination pathway is the formation of a carbonyl and alcohol compound:

$$RO_2 + R'O_2 \rightarrow R{-}OH + R'{=}O + O_2. \quad \text{(R3)}$$

In this reaction, both radicals lose an oxygen atom, and a hydrogen atom is transferred to the RO_2, forming the alcohol termination group. Preferences of RO_2 to form an alcohol or carbonyl compound are possible for individual reactions, but statistically carbonyl and alcohols should be formed with the same fractions. Since mass spectrometry can only determine formula composition, we cannot distinguish alcohols and hydroperoxides, which arise from RO_2 differing by one O atom. Therefore, details of balance of alcohol and carbonyl formation cannot be detected.

However, the formula composition can help to differentiate certain formation pathways. The $C_{10}H_{14}O_z$ family contains only carbonyl formed from a $C_{10}H_{15}O_x$ RO_2, while the alcohol will be part of the $C_{10}H_{16}O_z$ family. The $C_{10}H_{16}O_z$ family also contains the carbonyl produced

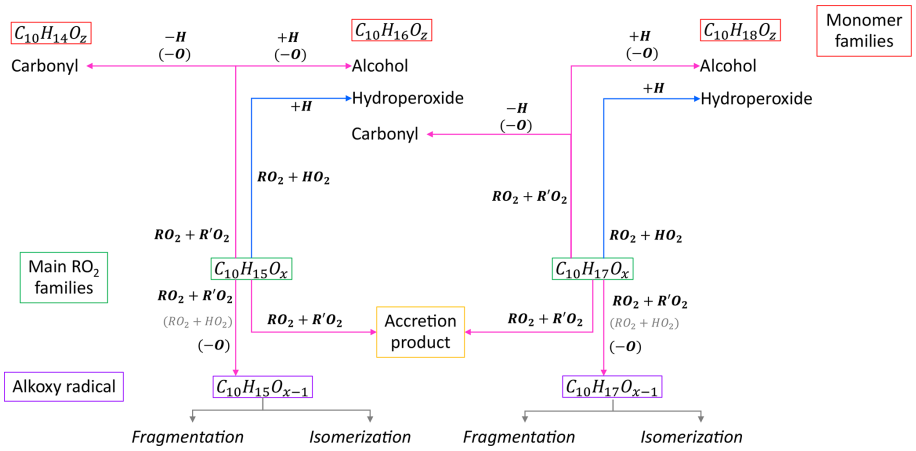

Figure 1. Overview of important reaction pathways of α-pinene RO_2 with other RO_2 and HO_2.

from the RO_2+$R'O_2$ monomer termination of $C_{10}H_{17}O_x$, while the alcohol from this RO_2 family will be found in the $C_{10}H_{18}O_z$ family. So, from a diagnostic point of view, $C_{10}H_{14}O_z$ as well as $C_{10}H_{18}O_z$ are uniquely related to a precursor radical family.

The classification of the formation pathways of the monomers is helpful to analyze the effect of the HO_2/RO_2 ratio shift in the experiments. Considering the termination pathways, a decrease in the $C_{10}H_{14}O_z$ family and an increase in the $C_{10}H_{18}O_z$ family are expected with increasing HO_2/RO_2 because of increasing termination by HO_2 and decreasing termination by RO_2. In the case of $C_{10}H_{18}O_z$, the increase in hydroperoxides is partially compensated by a decrease in the alcohol channel. For $C_{10}H_{16}O_z$, the situation is more complicated as it contains contributions from all termination pathways.

Besides closed-shell products, HOM-RO_2 can also form alkoxy radicals (HOM-RO). In general, alkoxy radicals (RO) are important intermediates in the oxidation scheme of organics and are formed via (Reaction R4) and probably also via (Reaction R5) for specific RO_2 (Jenkin et al., 2019):

$$RO_2 + R'O_2 \rightarrow RO + R'O + O_2, \quad \text{(R4)}$$

$$RO_2 + HO_2 \rightarrow RO + OH + O_2. \quad \text{(R5)}$$

In Reaction (R5), OH will be formed. The importance of Reaction (R5) compared to Reaction (R1) is still unclear in the literature, but functionalization of the RO_2 close to the peroxy functionality possibly enables this reaction (Iyer et al., 2018; Eddingsaas et al., 2012; Hasson et al., 2005; Jenkin et al., 2019). If Reaction (R5) is of negligible importance, the reaction scheme will simplify, and the effect of increased HO_2/RO_2 is easier to diagnose.

We are interested in the importance of alkoxy radical formation as (HOM)-RO tends to fragment, leading to the formation of smaller products (Vereecken et al., 2007). In the context of SOA formation, these fragments are less likely to contribute to SOA mass because of their higher volatility. Since alkoxy radicals are too unstable to be detected directly, we use two diagnosis tools to judge the importance of HOM-RO. Firstly, HOM-RO fragmentation can lead to HOM-RO_2 with less than 10 carbon atoms, which may also continue the autoxidation chain. Therefore, the abundance of HOM with less than 10 carbon atoms (HOM-Frag) indicates the importance of alkoxy steps. Secondly, with increasing functionalization, H shifts retaining the carbon backbone become more likely (Vereecken et al., 2007), which will lead to the generation of new C_{10}-HOM-RO_2. Such alkoxy peroxy steps can continue the autoxidation chain (Mentel et al., 2015). Interestingly, by coupling of an alkoxy and a peroxy step, the parity of the number of oxygen atoms in the HOM-RO_2 changes, while in pure autoxidation steps the oxygen parity remains the same. Therefore, a parity change of the oxygen number can be used as an indication of alkoxy step abundance (Kang, 2021).

In summary, we will use the changes in contribution and relative signal of the different families and classes to judge the impact of shifting from low to high HO_2/RO_2 on the α-pinene photooxidation pathway.

2.2 Control of α-pinene OH turnover

After the initial α-pinene photooxidation phase as a reference, CO was added to the oxidation system. The idea is to represent small, oxidized VOCs in the atmosphere that can produce HO_2 by reaction with OH (compare Schervish and Donahue, 2021). The presence of CO shifts the HO_2/RO_2 ratio, increasing the importance of the termination of RO_2 by HO_2. McFiggans et al. (2019) showed that one limiting factor in mixture experiments is oxidant scavenging: the products and their yields in mixed systems change, because there is less OH available to the individual VOCs. Thus, after the CO addition the OH production in the chamber was increased to compensate for the OH consumed by CO. The OH levels in the system before and after the CO addition were approxi-

mately the same, keeping the α-pinene OH turnover approximately constant. This OH adjustment ensures that the primary α-pinene chemistry was kept the same, avoiding effects by different oxidant levels and enabling a direct comparison.

However, since experiments could only be performed at *about* the same OH levels, a normalization by the actual α-pinene OH turnover is applied to the data. This compensates for the slight experimental imperfections and enables better comparison of experiment series with different boundary conditions. The turnover in steady state is given in Eq. (1). Here the subscript "SS" denotes steady-state condition for the concentrations of α-pinene and OH, and k_{OH} is the α-pinene OH reaction rate constant.

$$\text{turnover}_{\alpha\text{-pinene+OH}} = k_{OH} \cdot \left[\alpha\text{-pinene}\right]_{SS} \cdot [OH]_{SS} \quad (1)$$

This normalization also directly shows the yield of certain oxidation products or product groups per α-pinene consumed by OH.

2.3 Derivation of effect on condensable mass from gas-phase measurement

A simple proxy for the condensable mass from HOM products can be calculated from the steady-state HOM signals measured by the NO_3-CIMS, assuming condensation for all low-volatility HOM compounds and no back-evaporation into the gas phase. To only take low-volatility products into account, we used all detected formula compositions with $M > 230\,\text{g mol}^{-1}$ and weighted them with their molar mass. The reasoning behind this threshold can be found in Sect. 4.4. All contributions were summed up and normalized with the α-pinene OH turnover for the comparison between the low and high HO_2/RO_2 cases (Eq. 2).

$$\text{mass-weighted signal sum} = \frac{\sum_{i=0}^{i} S_i \cdot M_i}{\text{turnover}_{\alpha\text{-pinene+OH}}} \quad (2)$$

We also estimated the expected SOA mass formed using the calibration factor obtained for sulfuric acid for our NO_3-CIMS instrument in a calibration setup (see Supplement Sect. S1). From this, we calculated an upper boundary concentration of detected HOM compounds in the gas phase under the assumption that sulfuric acid clusters with nitrate at the collision limit, yielding maximum sensitivity (a common approach; see, for example, Ehn et al., 2014, and Pullinen et al., 2020).

The calculated gas-phase concentration was then used in the steady-state equation describing the relationship between gas- and particle-phase concentrations of a single compound i shown in Eq. (3).

$$m_{i,\text{seed}}(p) = \frac{m_{i,\text{seed}}(g) \cdot k_{\text{cond},i}}{k_{\text{particleLoss}} + k_{\text{evap},i}} \quad (3)$$

Equation (3) shows that the steady-state particle-phase (mass) concentration $m_{i,\text{seed}}(p)$ of compound i in the presence of seed particles in the chamber is only dependent on the steady-state gas-phase concentration $m_{i,\text{seed}}(g)$, the condensation rate and evaporation rate constants $k_{\text{cond},i}$ and $k_{\text{evap},i}$ of i (to and from the particles) and the particle-loss rate constant $k_{\text{particleLoss}}$ in the chamber. The condensation rate can be calculated (see Supplement Sect. S8), and the particle-loss rate constant was measured by observation of the particle loss in the chamber after ending the seed addition (details in the Supplement Sect. S2). The evaporation rate was assumed to be negligible for the investigated HOM compounds.

For the SOA yield calculation, we calculated a corrected organic mass m_{SOA} from the organic mass m_{AMS} measured by aerosol mass spectrometry (AMS) and the fraction expected to be lost on the seed particles compared to the overall loss on particles and chamber wall as shown in Eq. (4) (McFiggans et al., 2019).

$$m_{\text{SOA}} = m_{\text{AMS}} \cdot \frac{k_{\text{cond}} + k_{\text{wall}}}{k_{\text{cond}}} \quad (4)$$

In Eq. (4), we use the condensation rate constant k_{cond} calculated for one major HOM product ($C_{10}H_{16}O_7$) and the average HOM-Mon wall loss rate k_{wall}, which was determined by switching off the UV-C light and observing the decay of photooxidation products in the NO_3-CIMS. The wall loss determination, as well as SOA mass correction, was described before in Sarrafzadeh et al. (2016) and McFiggans et al. (2019).

3 Experimental methods

3.1 Chamber setup

Experiments were conducted in the Jülich SAPHIR-STAR chamber, which is the modern successor of the JPAC setup (Mentel et al., 2009). The basic concepts are the same as in JPAC, but each parameter is set, controlled and monitored in a program. The chamber was operated as a continuously stirred tank reactor. It is a borosilicate glass cylinder ($l = 2.5\,\text{m}, d = 1\,\text{m}$) with a volume of close to 2000 L, and all equipment inside the chamber is either glass or glass-coated steel (SilcoTek GmbH).

With an inflow of $32\,\text{L min}^{-1}$, the residence time in the chamber was approximately 61 min with a fan ensuring mixing within minutes. In contrast to the JPAC chamber, the stirring is conducted perpendicular to the cylinder axis, as opposed to coaxial. Chamber inflow is split into two humidified clean air flows (mixed from N_2 and O_2) of about equal volume: one with added oxidant (here O_3) and the other with added VOC and other trace gases (here α-pinene and CO). All experiments were performed at a relative humidity of 50 % and temperature of 20 °C. Temperature stability is ensured by the climate-controlled surroundings of the chamber.

α-Pinene (≥ 99 % purity, Sigma-Aldrich, Merck KGaA) was introduced via liquid injection with a syringe pump

(Fusion 4000, CHEMYX Inc.) into a heated glass bulb and flushed by a $1\,L\,min^{-1}$ N_2 stream into the chamber. CO was added from a gas bottle (10 % CO in N_2, Messer SE & Co. KGaA). Ozone was directly produced photolytically before injection with a self-built ozone generator.

OH is produced in the chamber by ozone photolysis using two UV-C lamps with a wavelength of 254 nm and subsequent reaction of $O(^1D)$ with water vapor. The lamps are mounted in closed quartz cylinders in the middle of the chamber, vertically to the cylinder axis, and light intensity can be varied with a movable shielding installed around the lamps. The shielding allows for an exact percentage of the lamp to be covered, thus controlling the amount of OH produced in the chamber.

The OH radical concentration after CO addition was adjusted by setting the shielding of the UV-C lamps and a slight adjustment of O_3 inflow. The applied $J(O^1D)$ values in different phases were calculated to be in the range of 0.8×10^{-3} to $2.4 \times 10^{-3}\,s^{-1}$.

In some of the experiments, ammonium sulfate ($\geq 99\,\%$ purity, Merck KGaA) seed particles were added to the system to provide a surface for the condensation of organic material. The aerosol was produced with a modified TSI atomizer (model 3076, TSI GmbH) and dried to 50 % relative humidity.

VOC concentrations in the chamber were measured using proton-transfer-reaction mass spectrometry (PTR-TOF-MS; Ionicon GmbH). CO_2, CO and H_2O (G2401 cavity ring-down spectrometer, Picarro Inc.); NO and NO_x (NCLD899, Eco Physics GmbH with a home-built photolytic converter); and O_3 (O342e, Envea GmbH) were additionally monitored. Particle distribution and concentration were measured with a condensation particle counter (CPC, model 3788, TSI GmbH) and a scanning mobility particle sizer (SMPS; model 3080, TSI GmbH) with a CPC (model 3788, TSI GmbH). The aerosol composition was measured with a high-resolution aerosol mass spectrometer (HR-TOF AMS; Aerodyne Inc.).

In all experiments, VOC, O_3 and SMPS + CPC sampling switched between inlet and outlet of the chamber to measure the input concentrations as well as the concentrations in the reactor. The flow control system of the chamber adapts to these switches so that the inflow into the chamber stays constant.

All results discussed here were observed under steady-state conditions when all parameters were constant. For each steady state, the OH concentration was calculated from the decay of α-pinene as described by Kiendler-Scharr et al. (2009). Equation (5) is derived from the mass balance of α-pinene at steady state. The steady-state OH concentration $[OH]_{SS}$ depends on the amount of α-pinene consumed by reaction with OH and the reaction with O_3, as well as the flush out.

$$[OH]_{SS} = \frac{\frac{F}{V} \cdot \frac{[VOC]_{in} - [VOC]_{SS}}{[VOC]_{SS}} - k_{O3} \cdot [O_3]_{SS}}{k_{OH}} \quad (5)$$

Here, F is the total flow and V the volume of the chamber. The subscript "SS" indicates steady-state concentrations, while $[VOC]_{in}$ represents the α-pinene concentration entering the chamber. k_{O3} and k_{OH} represent the reaction rate constants of α-pinene with the corresponding oxidant. We applied rate coefficients of $k_{OH} = 5.36 \times 10^{-11}\,cm^3\,s^{-1}$ (Atkinson and Arey, 2003) and $k_{O3} = 9.25 \times 10^{-17}\,cm^3\,s^{-1}$ (Cox et al., 2020) at 20 °C. The uncertainty of the OH calculation was estimated as 20 % by Wildt et al. (2014).

3.2 Experiment conditions

An overview of the experiments and their boundary conditions can be found in Table 1. Four experiments were performed in total, leading to one repetition of each studied condition. In two of the experiments, ammonium sulfate seeds were added, leading to a total particle surface in the chamber on the order of $8 \times 10^{-4}\,m^2\,m^{-3}$ and organic loadings of about $3\,\mu g\,m^{-3}$ in the photooxidation stage. In the unseeded experiments, no significant nucleation was observed, leading to pure gas-phase conditions. The *Exp2* experiment is a consecutive combination of a seeded followed by a non-seeded experiment to provide direct insight into the effect of the seed presence on the system.

As the OH radical is produced by photolysis of ozone and as α-pinene reacts with ozone, it is important to know the relative contribution of the α-pinene consumption by OH and by O_3. This is achieved by comparing the turnover of α-pinene with OH and O_3, respectively. The results can be found in Table 1. The listed results are for the low HO_2/RO_2 conditions, but nearly identical values were reached after the HO_2/RO_2 shift.

3.3 Experimental procedure

All experiments started with α-pinene ozonolysis followed by illumination with the UV-C lights to induce the reaction with OH. A general flow scheme of the experiment can be found in Fig. 2, together with one exemplary time series of the unseeded experiment (*Exp1*). After the photooxidation steady state, CO was added to the system. In the displayed *Exp1*, the OH level was adjusted in three steps to approach the same concentration as before the CO addition. First the UV-C light opening was adjusted and then O_3 was added, and the UV-C light opening was adjusted again. In some experiments initially the effect of CO on the unchanged system was observed before the adjustment of OH. In other experiments (*Exp2.2*, *Exp3*), the adjustment of the α-pinene OH turnover via ozone concentration and UV-C light opening were made simultaneously with the CO addition. Highlighted in green

Table 1. Overview of experimental conditions.

Name	Experiment description	$[VOC]_{in}$	$[CO]_{in}$	$[OH]_{ss}$ at low HO_2/RO_2	Contribution of OH to turnover at low HO_2/RO_2	Particle surface at low HO_2/RO_2	Organic mass concentration at low HO_2/RO_2
Exp1	*unseeded (1)*	10 ppbv	2.5 ppmv	4.8×10^6 cm^{-3}	80 %	–	–
Exp2.1	*seeded (1)*	10 ppbv	2.5 ppmv	1.1×10^7 cm^{-3}	92 %	8.7×10^{-4} m^2 m^{-3}	3.4 µg m^{-3}
Exp2.2	*unseeded (2)*	10 ppbv	2.5 ppmv	1.5×10^7 cm^{-3}	94 %	–	–
Exp3	*seeded (2)*	10 ppbv	2.5 ppmv	1.1×10^7 cm^{-3}	92 %	6.8×10^{-4} m^2 m^{-3}	2.7 µg m^{-3}

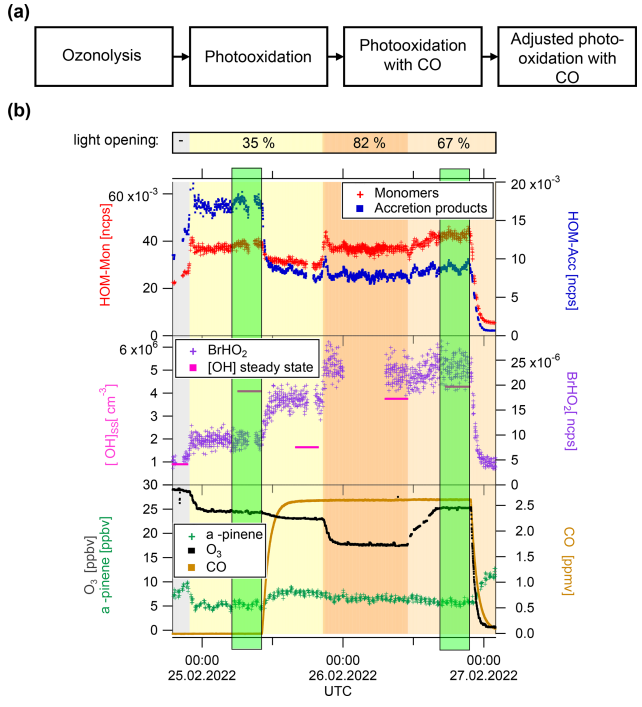

Figure 2. **(a)** Experiment flow scheme. **(b)** Exemplary time series of *Exp1*, showing HOM-Mon and HOM-Acc product sum (top panel); calculated OH concentration and $BrHO_2$ signal (middle panel), and ozone, α-pinene, and CO concentrations (bottom panel). Background color represents light intensity. Highlighted in green are the low HO_2/RO_2 steady state and the steady state at high HO_2/RO_2 (addition of CO and adjusted oxidant level).

are the steady states with the "same" OH concentration characterized by low and high HO_2/RO_2, which were used for analysis and interpretation.

3.4 Model calculation for HO_2/RO_2 ratio estimation

Box-model calculations were performed by applying the MCM v3.3.1 chemistry (Jenkin et al., 1997; Saunders et al., 2003) under the boundary conditions of the SAPHIR-STAR chamber. All calculations were performed with the institute software package EASY, which uses FACSIMILE to solve the differential equations (EASY Version 5.69b). More details about the model parameters can be found in the Supplement Sect. S3. The model calculations reproduced the primary observables α-pinene, O_3, CO and OH within the experimental uncertainties. The box-model results were used to characterize the HO_2/RO_2 ratio of the chemical systems, as no direct measurement of these parameters was available. The observed cluster signal $BrHO_2^-$ follows the modeled HO_2 concentration (Fig. 3).

The model predicts a shift of the HO_2/RO_2 ratio from about 0.01 to about 1 by CO addition and oxidant adjustment, an increase by 2 orders of magnitude. Owing to a lack of observations to verify model results, we will consider only the magnitude of HO_2/RO_2 here. The model results show that indeed a major shift from $RO_2 + RO_2$ to $RO_2 + HO_2$ reactions can be expected.

We further used the modeled RO_2 and HO_2 concentrations to estimate the relative importance of pathways for individual (observed) HOM-RO_2. For that, we applied two generic rate coefficients k_{RO2HO2} and k_{RO2RO2}. As the rate coefficient for the $RO_2 + HO_2$ termination to a hydroperoxide (k_{RO2HO2}), we used the value specified in the MCM (2.46×10^{-11} cm^3 s^{-1} at 20 °C (Jenkin et al., 1997; Saunders et al., 2003)). We chose a k_{RO2RO2} of 5×10^{-12} cm^3 s^{-1} as the approximated reaction rate of the $RO_2 + RO_2$ reactions. This value applies to all possible reactions (accretion product, monomer, and alkoxy formation) and is in the range of k_{RO2RO2} utilized by Roldin et al. (2019) in the PRAM model.

3.5 Determination of oxidized VOCs, HOMs and HO_2

Chemical ionization mass spectrometry (HR-TOF-CIMS) techniques were used to detect a range of gaseous compounds. For this, two atmospheric-pressure-interface time-of-flight mass spectrometers (APi-TOF-MS; Tofwerk AG) with different inlet systems were used simultaneously. General information about the APi-TOF-MS instrument can be found in Junninen et al. (2010).

A long TOF (LTOF, Tofwerk AG) (resolution of ∼8500 for peaks at $> m/z$ 200) was coupled with the multi-scheme

ionization inlet (MION; Karsa Oy). The setup of the inlet is described in detail by Rissanen et al. (2019). The distinctive feature of the MION inlet is the switching between two reagent ions. Here, nitrate was used to detect closed-shell HOMs, as well as HOM-RO_2. Bianchi et al. (2019) suggested to define HOMs as products stemming from autoxidation containing more than six oxygen atoms. In our overall analysis, we decided to also include fragments and monomers containing five or in a few cases four oxygens (see the peak list in Supplement Sect. S5) as we are interested to see if the importance of these less oxidized (but still with NO_3-CIMS detectable) products increases at higher HO_2/RO_2. However, in all considerations regarding SOA formation, we furthermore set a molar weight threshold which automatically excluded any products with less than six oxygens.

As the second reagent ion, bromide was used to detect less oxidized products and the HO_2 radical (Albrecht et al., 2019; Sanchez et al., 2016). The nitrate ion source had a reaction time of 600 ms, while the bromide ion source had a shorter reaction time of 60 ms. For all experiments, an inlet flow of 10 L min^{-1} was used, and the ionization scheme was switched every 10 min.

In the data evaluation, the first step was the separation of the time series of the two reagent ions. The data were subsequently processed with Tofware (Version 3.2.3, Tofwerk AG), using the high-resolution time series workflow. No transmission correction was performed as previous measurements showed an approximately flat relative transmission curve in the mass region of interest. The analyte signals were normalized with the reagent ion signal (NO_3^- and $HNO_3NO_3^-$ for nitrate and Br^- and BrH_2O^- for bromide).

Since no direct HO_2 calibration was available, the HO_2 signal in the Br-MION-CIMS was used to compare the levels of HO_2 relative to each other in the different phases of the experiment. The comparison of the measured HO_2 signal to the modeled HO_2 concentration shows a good linear relation between the model predictions and observations.

Figure 3 illustrates this for the example of the *Exp2* experiment. A background signal of around $\sim 1 \times 10^{-5}$ is observed as soon as VOC and ozone are present in the reactor. The background HO_2 signal was not observed when only O_3 or only VOC were in the system. As shown by the MCM modeling results, HO_2 production of this strength is not expected in the α-pinene ozonolysis phase, but this background phenomenon was observed before (Albrecht et al., 2019) and is not fully understood.

For the HOM molecules measured by the NO_3-MION-CIMS, the relative changes between different experiment phases are compared. For all detected HOM products, the same detection sensitivity is assumed. Hyttinen et al. (2018) showed in quantum chemical calculations that HOMs containing six or more oxygen atoms have comparable sensitivity with the nitrate reagent ion. At this degree of oxidation, it can be expected that the HOMs already contain multiple hydroperoxyl and/or hydroxy functional groups (Bianchi et al., 2019) prior to the termination step, making it unlikely that the sensitivity is strongly influenced by the termination group. Thus, the signal strength reflects the correct ranking of the observations, and relative comparisons do not require calibration. Pullinen et al. (2020) studied the mass balance between condensable HOMs and formed particle mass and were able to find closure within a factor of 2.

A second CI-APi-TOF was used to measure less oxidized species. It was configured with a CI inlet based on the design of Eisele and Tanner (1993) coupled to a TOF-MS (HTOF Tofwerk AG, resolution ~ 2700 for peaks at $> m/z$ 200) and was operated in positive mode with propylamine ($C_3H_7NH_2$, Sigma-Aldrich, purity ≥ 99 %) to detect the early-generation RO_2 and oxidation products (Berndt et al., 2018). The propylamine was purified and added as an amine–N_2 mixture (flow: 0.12 mL min^{-1}) to the 30 L min^{-1} sheath flow. Furthermore, the sheath flow air is humidified to optimize ionization. The instrument sampled 0.1 L min^{-1} from the chamber, which was diluted with 9.9 L min^{-1} for a sample flow of 10 L min^{-1}. The dilution was necessary to reduce depletion of the primary ion (Hantschke, 2022).

4 Results and discussion

In order to understand the effect of HO_2/RO_2 on the gas-phase product composition, we will present and compare two cases: the steady state without CO (low HO_2/RO_2) and the steady state with CO addition and OH adjustment by $J(O^1D)$ and O_3 (high HO_2/RO_2). The modeling results predicted HO_2/RO_2 of about 1/100 and of about 1/1 for these two cases, respectively. The modeled concentrations can be found in Supplement Sect. S4. The modeling results show that the HO_2/RO_2 ratio changes by 2 orders of magnitude, because $[RO_2]$ was reduced by about a factor of 3, while $[HO_2]$ was increased by a factor of 30. Consequently, HO_2 reactions were almost negligible at low HO_2/RO_2 while $RO_2 + RO_2$ reactions can still contribute at high HO_2/RO_2.

HO_2/RO_2 ratios of around 1 are highly relevant for atmospheric conditions with significant OH oxidation, though it should be kept in mind that in atmospheric conditions the methyl peroxy radical and other small RO_2 contribute a significant portion to the total of peroxy radicals (Khan et al., 2015). Field studies reporting HO_2 and RO_2 measurements for different environments can be found in the Supplement Table S5. These exemplary studies show that HO_2/RO_2 ratios around 1 are relevant in remote to urban environments with different VOC sources and NO_x levels.

Assuming correctly modeled $[HO_2]$ and $[RO_2]$, we calculated the competition between HO_2 and RO_2 reactions for each (observed) RO_2 expressed in the form of pseudo-first-order rate coefficients in $k_{RO2HO2} \cdot [HO_2]$ or $k_{RO2RO2} \cdot [RO_2]$. Herein $[RO_2]$ is the sum of all RO_2 species as defined in the MCM v3.3.1. For all experiments, the results of

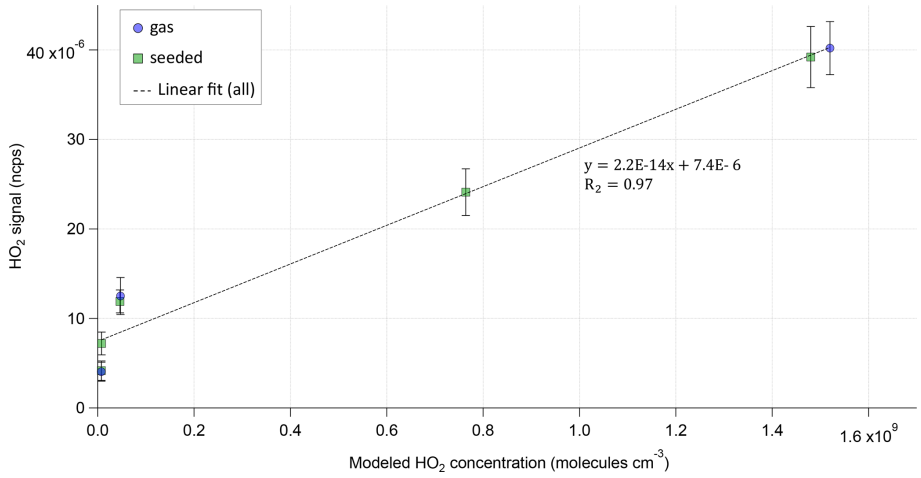

Figure 3. Modeled HO_2 concentration vs. normalized HO_2 signal for each steady state of Exp2. HO_2 is measured as the $BrHO_2$ cluster and is normalized with the sum of the reagent ion Br^- and its water cluster. The dotted line shows the linear fit to all (gas phase and seeded) measurement points.

our calculations indicate that the sink for HOM-RO_2 is dominated by RO_2+ RO_2 reactions at low HO_2/RO_2 (∼ 97 % contribution), while at high HO_2/RO_2 RO_2+ HO_2 contributed ∼ 80 %. As the rate coefficients are not well known and as we cannot verify the modeling results for HO_2 and RO_2, our calculations serve solely as an indication of expected trends in the chemical system.

4.1 Impact on overall HOM formation

The top panel of Fig. 2 shows the time series of HOM-Mon and HOM-Acc products. The HOM-Mon signal recovers after the oxidant adjustment, while the HOM-Acc signal is significantly suppressed at high HO_2/RO_2. This indicates that the shift from low to high HO_2/RO_2 substantially impacts the termination reactions, shifting formation from the HOM-Acc product channel (RO_2+RO_2) to the HOM-Mon channel.

An overview of the results for the product classes defined in the method section is shown in Fig. 4. Plotted are the average ratios of signal in the NO_3-CIMS in the high HO_2/RO_2 steady state compared to the low HO_2/RO_2 steady state. For better comparison, all experiment phases were normalized to the actual α-pinene OH turnover. The overall HOM-signal was lower at high HO_2/RO_2, showing a reduction of about 20 %. Most distinctive, the HOM-Acc compounds were strongly reduced by about 60 %. A reduction of HOM-Acc by addition of CO was observed before by McFiggans et al. (2019); however, there the OH concentration was not kept constant. The HOM-Frag signal ($5 \geq C < 10$) also shows a reduction of about 20 %. At high HO_2/RO_2, the C_{10}-HOM-RO_2 signal was also reduced significantly by about 40 %.

The HOM-Mon signal level remained about the same at low and high HO_2/RO_2. Without changes in the rates and contributions of the different termination reactions, the observed reduction in the HOM-RO_2 precursors should lead to nearly the same reduction in HOM-Mon. However, the decrease in accretion product formation and fragmentation should lead to an increase in HOM-Mon. The presence of HO_2 could reduce the alkoxy formation and thus fragmentation of HOM-RO_2. This missing sink could lead to an additional HOM-Mon source compared to the low HO_2/RO_2 case. However, the distribution of the product classes at low and high HO_2/RO_2 (Fig. 5) shows that contributions are shifted from HOM-Acc to HOM-Mon, while the contribution of HOM-Frag remains constant. Each HOM-Acc is formed from one HOM-RO_2 (HOM-RO_2+ RO_2) or potentially even two HOM-RO_2 compounds (HOM-RO_2+ HOM-RO_2) and therefore each HOM-Acc not formed will lead to at least one HOM-Mon.

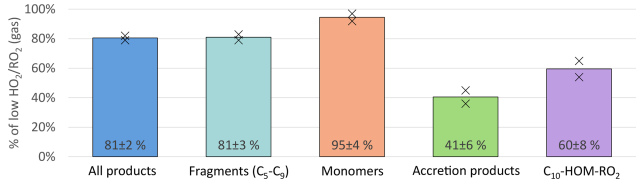

Figure 4. Overview of average, relative change in product classes detected in NO_3-CIMS between low and high HO_2/RO_2 cases (both normalized to α-pinene OH turnover) for unseeded experiments. Bars represent the average of the two experiments; markers represent individual experiments.

Further changes in the product distribution become evident when considering the individual HOM-Mon families as shown in Fig. 6. The $C_{10}H_{15}O_x$ peroxy radical family and the related $C_{10}H_{14}O_z$ family (carbonyl compounds) show the strongest suppression with a decrease of about 40 % at high HO_2/RO_2. For the $C_{10}H_{17}O_x$ peroxy radical family,

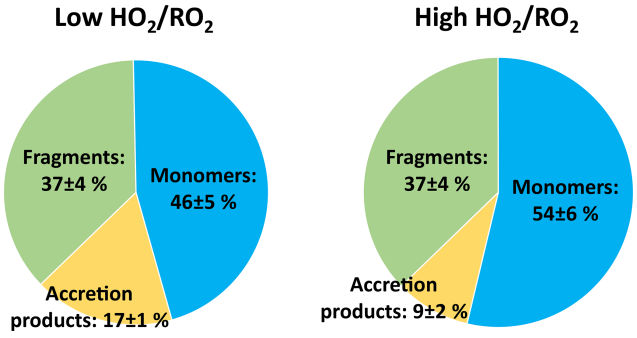

Figure 5. Average contribution of the closed-shell product classes to overall HOM-product signal in the low and high HO_2/RO_2 cases (unseeded experiments).

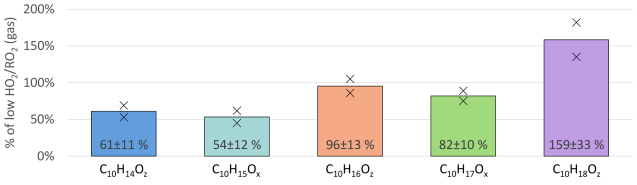

Figure 6. Overview of average, relative change in monomer families detected in NO_3-CIMS between low and high HO_2/RO_2 cases (both normalized to α-pinene OH turnover) for unseeded experiments. Bars represent the average of the two experiments; markers represent individual experiments.

the suppression was less pronounced with a 18 % reduction. In contrast, the $C_{10}H_{16}O_z$ family remained about the same, while the $C_{10}H_{18}O_z$ family showed a strong increase at high HO_2/RO_2.

The suppression of C_{10}-HOM-RO_2 of only about 40 % compared to the reduction of overall [RO_2] by $\sim$ 70 % in the model calculations (for the modeled concentrations, see the Supplement Sect. S4) shows that in many instances the autoxidation is too efficient to be out-competed by the $RO_2 + HO_2$ termination reaction, which is several times faster than $RO_2 + RO_2$ reactions.

Furthermore, the signal-weighted O/C ratio of the monomer class does not change between low and high HO_2/RO_2 (0.70 ± 0.01). If the HO_2 termination would interrupt the autoxidation chain, a lower oxidation level would be expected at high HO_2/RO_2. The unchanged oxidation level and the suppression of HOM-Acc indicate that the average autoxidation rate must be faster than $k_{RO2HO2} \cdot$ [HO_2], while the average accretion rate for $k_{HOM-RO2+RO2} \cdot$ [RO_2] must be slower. In conclusion, the change in HO_2/RO_2 should essentially impact the distribution of the HOM-RO_2 termination products.

4.2 Impact on HOM-RO_2

C_{10}-HOM-RO_2 compounds are key to understand the changes in the HOM product distribution. Therefore, we will first discuss the changes in the HOM-RO_2 products and then the changes in the closed-shell products.

The C_{10} peroxy radical class consists of the $C_{10}H_{15}O_x$ and $C_{10}H_{17}O_x$ families, which were reduced to 54 % and 82 %, respectively, when comparing the high and low HO_2/RO_2 cases (Fig. 6, light blue and green bars). The observed reduction in C_{10}-HOM-RO_2 is significantly smaller than the overall RO_2 concentration reduction predicted by the MCM model results (reduction to $\sim$ 30 %). In the following paragraphs, we present a plausibility consideration to assess if these observed changes are consistent with our expectations from modeling results and reaction rates.

The change in the steady-state concentration of a compound is always defined by the changes in its sources and sinks. The source of a HOM-RO_2 is the intramolecular reaction of a precursor RO_2; thus, the HOM-RO_2's source is reduced if the steady-state concentration of the precursor RO_2 is reduced. However, assuming the source term of the precursor RO_2 is the same in low and high HO_2/RO_2 (due to the constant α-pinene OH turnover) and the precursor RO_2's sink term is dominated by the fast autoxidation in both cases, then the RO_2's steady-state concentration would not be significantly changed. This consideration is only applicable for RO_2 where autoxidation dominates the sink term at low and high HO_2/RO_2. However, the unchanged oxidation level of the HOM-Mon indicates that once the autoxidation is initiated it out-competes the possible termination reactions.

In this case, the change in steady-state concentration of the HOM-RO_2 will be defined by the changes in the sink terms. Owing to the faster reaction of $RO_2 + HO_2$ compared to $RO_2 + RO_2$ the chemical sink for all RO_2 including HOM-RO_2 with slower autoxidation rates increased, which leads to a reduction in the steady-state concentration of RO_2 in general, despite holding the primary RO_2 source term constant.

For steady-state conditions, we can estimate the expected effect on the RO_2 ratio between high and low HO_2/RO_2 conditions for those HOM-RO_2 with production directly linked to the primary production ($k_{OH} \cdot$ [OH] $\cdot$ [α-pinene]) with negligible further autoxidation. The necessary equations and assumptions can be found in Supplement Sect. S7. We assume the same primary production at low and high HO_2/RO_2 and that the reaction with HO_2, the reaction with RO_2 and the wall loss are the only significant loss pathways. At high HO_2/RO_2, a reduction to 80 % is expected if the chosen bulk rate constants are used ($k_{RO2HO2} = 2.46 \times 10^{-11}$ cm^3 s^{-1} at 20 °C (Jenkin et al., 1997; Saunders et al., 2003); $k_{RO2RO2} = 5.0 \times 10^{-12}$ cm^3 s^{-1}). A reduction to 60 % is expected if k_{RO2HO2} is around 7 times faster than k_{RO2RO2} ($k_{RO2RO2} = 3.3 \times 10^{-12}$ cm^3 s^{-1}). These reductions are in the range of what is observed for the C_{10}-HOM-RO_2. Of course, the approach of using generalized bulk rate constants is limited, but the resulting values for k_{RO2RO2} were clearly within the range of rate coefficients expected for HOM-$RO_2 + RO_2$ reactions (Roldin et al., 2019), showing that the increased chemical sink is a plausible explanation for our observations.

The $C_{10}H_{15}O_x$ family is on average reduced by around 30 % more than the $C_{10}H_{17}O_x$ family (see Fig. 6). $C_{10}H_{15}O_x$ peroxy radicals are either formed by sequential oxidation of α-pinene, e.g., from oxidation products like pinonaldehyde, or directly from α-pinene via the H-abstraction pathway (Shen et al., 2022). Formation of pinonaldehyde and even more so HOM formation via the H-abstraction channel involve alkoxy steps. However, alkoxy radicals should be reduced at high HO_2/RO_2 since they are mainly formed by RO_2+RO_2 reactions in the absence of NO_x. Thus, missing source terms add to the increased chemical sink by HO_2 for $C_{10}H_{15}O_x$ peroxy radicals.

Amine CIMS measurements enabled detection of the formula composition $C_{10}H_{16}O_2$ (e.g., pinonaldehyde). $C_{10}H_{16}O_2$ was reduced on average to $70\,\% \pm 1\,\%$ at high HO_2/RO_2 compared to low HO_2/RO_2. This supports that a fraction of the $C_{10}H_{15}O_x$ radical decrease at high HO_2/RO_2 arose from suppression of $C_{10}H_{16}O_2$ first generation products. In addition, a further suppression of HOM formation via the H-abstraction channel is likely. It should be noted that the reduction of $C_{10}H_{16}O_2$ is smaller than that expected by the MCM model results. Modeling results can be found in Supplement Sect. S4. This might indicate that HO_2 can also enable alkoxy radical steps to a certain degree as summarized by Jenkin et al. (2019) and postulated by e.g., Eddingsaas et al. (2012) as a source of pinonaldehyde in HO_2 dominated systems.

According to the model calculations, the pseudo-first-order rate coefficient $k_{RO2HO2} \cdot [HO_2]$ is expected to be about $0.04\,s^{-1}$ for the RO_2+HO_2 reaction at high HO_2/RO_2. Consequently, only such HOM-RO_2 with autoxidation rates of $\leq 0.04\,s^{-1}$ will be significantly lost by reaction with HO_2 at the higher HO_2 concentrations. However, typical isomerization rates of peroxy radicals in autoxidation are on the order of $0.1\,s^{-1}$, and many are faster (Piletic and Kleindienst, 2022; Berndt, 2021). Therefore, reduction in a HOM-RO_2 is only expected when the faster termination rate of $k_{RO2HO2} \cdot [HO_2]$ can compete with the autoxidation rate, i.e. when the autoxidation slows as the degree of oxidation increases on the specific HOM-RO_2. This consideration shows that the smaller reduction in HOM-RO_2 compared to the less oxidized RO_2 in the model is compatible with fast autoxidation reactions that are missing in the MCM.

The increase in chemical sink strength by going from RO_2 termination to HO_2 termination is the main expected reason for the decrease in $C_{10}H_{17}O_x$. As discussed, the $C_{10}H_{15}O_x$ family is subject to an additional decrease in the precursors due to the alkoxy steps necessary in the formation pathway. Since $C_{10}H_{15}O_x$ compounds were the main contributors to the C_{10}-HOM-RO_2 class, their stronger reduction is reflected in the overall reduction of C_{10}-HOM-RO_2.

4.2.1 Contribution of $C_{10}H_{15}O_x$ and $C_{10}H_{17}O_x$ families to HOM-RO_2

In the unseeded, pure gas-phase experiments, the contribution of the $C_{10}H_{17}O_x$ family to the C_{10}-HOM-RO_2 class is $23\,\% \pm 2\,\%$ on average in the low HO_2/RO_2 case. In the high HO_2/RO_2 case, the contribution increases to $31\,\% \pm 4\,\%$ on average. As discussed above, the suggested pathways to $C_{10}H_{15}O_x$ HOM-RO_2 may be additionally suppressed due to a decrease in alkoxy steps at high HO_2/RO_2, reducing the entry channel into $C_{10}H_{15}O_x$ HOM-RO_2.

Nevertheless, the contribution of $C_{10}H_{15}O_x$ is substantial in both experiment stages. Kang (2021) and Shen et al. (2022) reported that, in the photooxidation of α-pinene, the HOM-RO_2 compounds detected by NO_3-CIMS are dominated by the $C_{10}H_{15}O_x$ family, while $C_{10}H_{17}O_x$ formation is the main expected OH reaction pathway described in the literature (Berndt, 2021; Berndt et al., 2016; Xu et al., 2019).

This hints towards an effective pathway to HOM via $C_{10}H_{15}O_x$. A reason may be the fast opening of both carbon rings in the bicyclic α-pinene (Shen et al., 2022) or a four-ring opening in pinonaldehyde or similar compounds for easy autoxidation. From our observations, increasing the HO_2/RO_2 ratio does increase the relative importance of the $C_{10}H_{17}O_x$ family, but the change is less than 10 % in contribution.

Contribution of the two peroxy radical families to the HOM formation is also reflected in the composition of C_{20} HOM-Acc. Figure 7 shows the average contributions of the $C_{20}H_{30}O_z$, $C_{20}H_{32}O_z$ and $C_{20}H_{34}O_z$ families in the low and high HO_2/RO_2 cases. Although the absolute amount of HOM-Acc was suppressed by 60 % the family distribution was similar, $C_{20}H_{32}O_z$ dominated, while $C_{20}H_{30}O_z$ was lowest. $C_{20}H_{30}O_z$ is formed from two members of the $C_{10}H_{15}O_x$ family, while $C_{20}H_{34}O_z$ is formed by two members of the $C_{10}H_{17}O_x$ family. $C_{20}H_{32}O_z$ is then a combination of a $C_{10}H_{15}O_x$-RO_2 and $C_{10}H_{17}O_x$-RO_2.

Families that require one or two $C_{10}H_{17}O_x$ peroxy radicals for their formation have a higher contribution than the $C_{10}H_{17}O_x$ family's contribution to C_{10}-HOM-RO_2. Here, it is important to note that not only HOM-RO_2 can participate in HOM-Acc formation but also traditional, less oxidized RO_2 radicals (Berndt et al., 2018; Pullinen et al., 2020; McFiggans et al., 2019), which are not detectable by NO_3-CIMS. However, more oxidized peroxy radicals exhibit faster accretion rates (Berndt et al., 2018).

The large contributions of $C_{20}H_{32}O_z$ and $C_{20}H_{34}O_z$ thus clearly show the general importance of the $C_{10}H_{17}O_x$ peroxy radicals. The largest fraction, the $C_{20}H_{32}O_z$ family, indicates the importance of HOM-$C_{10}H_{15}O_x$ and a high abundance of less oxidized $C_{10}H_{17}O_x$ peroxy radicals. Less oxidized $C_{10}H_{17}O_x$-RO_2 compounds were recently measured by Berndt (2021). The fraction of $C_{20}H_{34}O_z$ is smaller because their formation requires HOM-$C_{10}H_{17}O_x$ radicals which are less abundant compared to HOM-$C_{10}H_{15}O_x$,

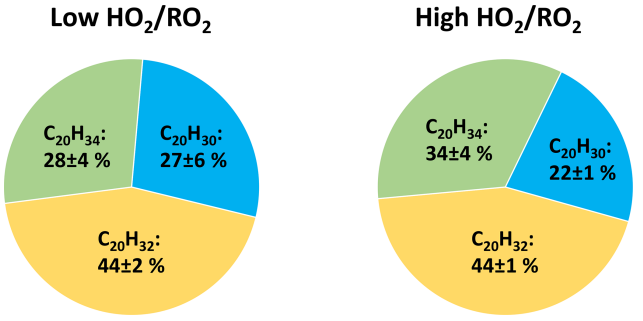

Figure 7. Average contribution of the $C_{20}H_{30}O_z$, $C_{20}H_{32}O_z$ and $C_{20}H_{34}O_z$ families to the C_{20} HOM-Acc group signal in the low and high HO_2/RO_2 cases (unseeded experiments). Not pictured is $C_{20}H_{28}O_z$ due to its negligible signal (contribution $\sim 1\,\%$).

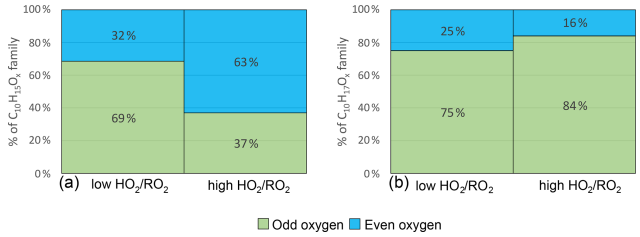

Figure 8. Average contribution of O_{odd} and O_{even} to the HOM-RO_2 families $C_{10}H_{15}O_x$ **(a)** and $C_{10}H_{17}O_x$ **(b)** signal in the low and high HO_2/RO_2 cases (unseeded experiments).

while the small fraction of $C_{20}H_{30}O_z$ indicates that, despite the importance of HOM-$C_{10}H_{15}O_x$, less oxidized $C_{10}H_{15}O_x$ are less important.

These results indicate the importance of mixed HOM-Acc formation by cross-reactions of HOM-RO_2 and a less oxidized RO_2. The importance of mixed HOM-Acc is supported by the relatively small fractions of HOM-Acc products with very high oxygen numbers, which more likely stem from HOM-RO_2+HOM-RO_2. For example, C_{20}-HOM-Acc compounds with 12 or more oxygen atoms contribute only around 30 % (low HO_2/RO_2: 26 % ± 4 %; high HO_2/RO_2: 31 % ± 2 %) of the signal in the product group.

Although the effect of the changed HO_2/RO_2 ratio is small, a tendency to higher $C_{20}H_{34}O_z$ contribution was observed. This is consistent with the observation of a slightly higher $C_{10}H_{17}O_x$ contribution to the C_{10}-HOM RO_2. The stronger suppression of the $C_{10}H_{15}O_x$ family at high HO_2/RO_2 is the first indication for, and can be explained by a reduction in the alkoxy radical formation.

4.2.2 Impact on HOM-alkoxy radical formation

Alkoxy radicals (RO) are the second important radical type in the oxidation chain of α-pinene. RO compounds cannot be detected directly as they are highly unstable and thus have very low concentrations. However, as explained in Sect. 2.2 the parity change in the HOM-RO_2 families can be used as a diagnosis tool for the abundance of alkoxy steps (Kang, 2021). A second indicator for alkoxy steps is the abundance of HOM products with less than 10 carbon atoms.

Figure 8 shows the average contribution of $C_{10}H_{15}O_x$ and $C_{10}H_{17}O_x$ with an even and odd number of oxygens at low and high HO_2/RO_2. $C_{10}H_{15}O_x$ radicals with an even number of oxygens contribute on average 32 % at low HO_2/RO_2. For $C_{10}H_{15}O_x$, the autoxidation chain is expected to start from an even number of oxygens either from $C_{10}H_{15}O_4$ (pinonaldehyde-like) (MCM v3.3.1 (Jenkin et al., 1997; Saunders et al., 2003) or from $C_{10}H_{15}O_2$ ($C_{10}H_{16}$ H abstraction) (Berndt, 2021; Shen et al., 2022). Therefore, without the involvement of an alkoxy step, the parity of the oxygen number in the observed $C_{10}H_{15}O_x$ HOM-RO_2 is expected to be even. Due to the average contribution of $C_{10}H_{15}O_{odd}$ of 69 %, we conclude that at least one alkoxy step (or any odd number of alkoxy steps) must have taken place in most of the cases at low HO_2/RO_2.

At high HO_2/RO_2, $C_{10}H_{15}O_{even}$ contributed 63 %, and the $C_{10}H_{15}O_{odd}$ contribution was reduced to 37 %. This demonstrates a change in the number of alkoxy steps along the formation pathway of the observed HOM-RO_2 radicals. The increased contribution of $C_{10}H_{15}O_{even}$ at high HO_2/RO_2 lets us infer an even number of alkoxy steps as more common (0, 2, 4, ...). In the simplest case, one alkoxy step takes place at low HO_2/RO_2 due to HOM-RO formation from HOM-RO_2+RO_2 reactions, while no alkoxy steps take place at high HO_2/RO_2, because HOM-RO_2+HO_2 produces none or less HOM-RO than HOM-RO_2+RO_2.

For $C_{10}H_{17}O_x$, the entry channel into autoxidation is $C_{10}H_{17}O_3$ with an odd number of oxygen atoms. Therefore, in autoxidation without alkoxy steps the oxygen parity is expected to be odd. At low HO_2/RO_2 $C_{10}H_{17}O_{odd}$ species contribute 75 % to the total $C_{10}H_{17}O_x$ signal indicating that either none or an even number (2, 4, ...) of alkoxy steps occurred. At high HO_2/RO_2 the odd contribution increases to 84 % (see Fig. 8). This result could indicate a low occurrence of alkoxy steps even at low HO_2/RO_2, with a further decrease in alkoxy formation at high HO_2/RO_2. However, the observed shift is minor.

In any case, the different responses of the $C_{10}H_{15}O_x$ and $C_{10}H_{17}O_x$ families to the reduction of HOM-RO_2 formation from HOM-RO_2+RO_2 at high HO_2/RO_2 indicate that there could be fundamental differences in the autoxidation chains of $C_{10}H_{15}O_x$ and $C_{10}H_{17}O_x$ (or the limit of the parity analysis). The parity analysis indicates a decrease in alkoxy steps at high HO_2/RO_2, but it cannot be directly inferred with certainty. However, the decrease in alkoxy steps at high HO_2/RO_2 is supported by the observation of changes in HOM-Frag products.

On average the sum of all HOM-Frag products (detected compounds with $5 \geq C < 10$ by NO_3-CIMS) showed a reduction of around 20 % (unseeded experiments; see Fig. 4). Further trends become recognizable when separating the species

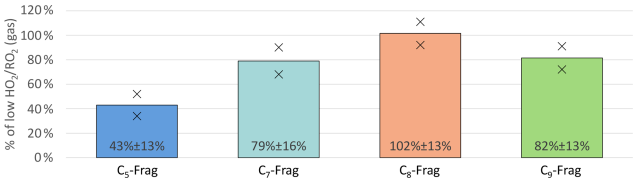

Figure 9. Overview of average, relative change in C_5, C_7, C_8 and C_9 fragment groups detected in NO_3-CIMS between high and low HO_2/RO_2 cases (both normalized to α-pinene OH turnover) for unseeded experiments. Bars represent the average of the two experiments; markers represent individual experiments.

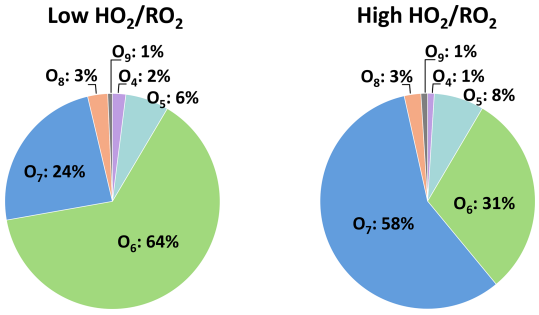

Figure 10. Average contribution of the individual compounds to the $C_{10}H_{18}O_z$ family signal at low and high HO_2/RO_2 (unseeded experiments).

according to their carbon number. Figure 9 shows the C_5, C_7, C_8 and C_9 HOM-Frag compounds at high HO_2/RO_2 compared to the low HO_2/RO_2 case, normalized to the α-pinene OH turnover. The fragment group with C_6 compounds is not included, as it contributed less than 5 % of the fragment signal and contained few detected compounds.

Figure 9 shows a significant reduction in HOM-Frag with shorter carbon chain length: C_5 HOM-Frag compounds are reduced by around 60 % compared to the low HO_2/RO_2 case. When we assume that the fragmentation of C_{10} compounds happens in consecutive steps via scission of HOM-RO radicals (analogously to the MCM), this observation is in accordance with decreasing importance of alkoxy radical formation at high HO_2/RO_2.

Overall, all observations indicate strong involvement of RO in HOM formation as well as a reduced, but still significant, involvement of RO at high HO_2/RO_2, when HO_2 chemistry dominates. This is supported by the change of the oxygen parity in C_{10}-HOM-RO_2 and the decrease of fragmentation products, especially with lower carbon number, as well as the only moderate reduction in the observed $C_{10}H_{16}O_2$ product (pinonaldehyde) and the still substantial importance of the $C_{10}H_{15}O_x$ HOM-RO_2 family at high HO_2/RO_2.

4.3 Impact on carbonyl and hydroperoxide formation

Increased HO_2/RO_2 should shift the product distribution by reduction of alcohol and carbonyl compounds from the so-called molecular channel in the RO_2+RO_2 reaction (see Reaction R3) in favor of hydroperoxide formation from RO_2+HO_2 termination (Reaction R1). This effect can be best observed in the $C_{10}H_{18}O_z$ family, which contains the hydroperoxide and alcohol termination products arising from $C_{10}H_{17}O_x$. $C_{10}H_{18}O_z$ significantly increased to, on average, 159 % (see Fig. 6). This supports an increased hydroperoxide formation but with some uncertainty due to the alcohol termination products from $C_{10}H_{17}O_x$ (by reaction with RO_2). To elucidate this further, the contribution of individual species to the $C_{10}H_{18}O_z$ family was examined.

Formation of an alcohol via the molecular path (Reaction R3) leads to the loss of one oxygen atom compared to the precursor $C_{10}H_{17}O_x$ radical, while in the hydroperoxide formation (Reaction R1) the oxygen number remains the same. The most abundant member of the $C_{10}H_{17}O_x$ family was $C_{10}H_{17}O_7$ with a contribution of 72 % ± 6 % at low HO_2/RO_2 and a contribution of 82 % ± 1 % at high HO_2/RO_2. $C_{10}H_{17}O_7$ terminates to $C_{10}H_{18}O_z$ products either as an alcohol with sum formula $C_{10}H_{18}O_6$ or as a hydroperoxide with sum formula $C_{10}H_{18}O_7$. These products have additional sources from $C_{10}H_{17}O_6$ and $C_{10}H_{17}O_8$, but due to the dominant contribution of $C_{10}H_{17}O_7$ to the $C_{10}H_{17}O_x$ family we expect any other production channels to be of minor importance.

Figure 10 shows the HOM product distribution within the $C_{10}H_{18}O_z$ family at low and high HO_2/RO_2. The sum of the O_6 and O_7 product did not change significantly in the two regimes (about 88 %), showing that these are the major products and agreeing well with the observation of $C_{10}H_{17}O_7$ being the major $C_{10}H_{17}O_x$ HOM-RO_2. At low HO_2/RO_2, the O_6 product has a larger contribution of 64 % ± 8 %, while at high HO_2/RO_2 ∼ 30 % of signal is shifted to the O_7 product. This shows that the increase in $C_{10}H_{18}O_z$ is matched with an increase in hydroperoxide formation.

An indicator for carbonyl formation is the $C_{10}H_{14}O_z$ family as it only contains the carbonyl products arising from $C_{10}H_{15}O_xRO_2$. The $C_{10}H_{14}O_z$ family was reduced on average to 61 % at high HO_2/RO_2; however, this decrease matches the decrease in the $C_{10}H_{15}O_x$ precursor family. If the reaction of a $C_{10}H_{15}O_x$-HOM-RO_2 with a second RO_2 were the main formation pathway for $C_{10}H_{14}O_z$, a stronger reduction would be expected as both precursor species were decreased significantly. Instead, it appears that $C_{10}H_{14}O_z$ is mainly impacted by the decrease in $C_{10}H_{15}O_x$ as their reductions are similar. A possible explanation could be that intramolecular termination is a major reaction pathway for $C_{10}H_{15}O_x$-RO_2, forming $C_{10}H_{14}O_x$ carbonyls. Intramolecular termination of the autoxidation chain has been discussed in the literature for different VOCs (Shen et al., 2021; Guo et al., 2022). Rissanen et al. (2014) discussed the possible importance of the unimolecular termination via an H shift, followed by formation of a carbonyl functional group and

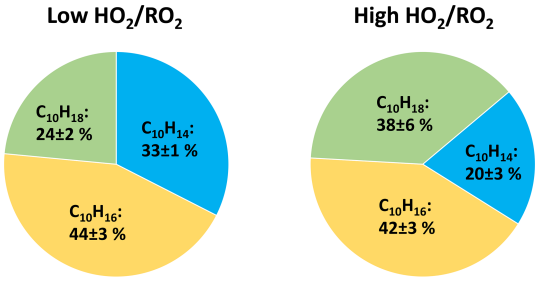

Figure 11. Average contribution of the $C_{10}H_{14}O_z$, $C_{10}H_{16}O_z$, and $C_{10}H_{18}O_z$ family to the monomer class signal at low and high HO_2/RO_2 (unseeded experiments).

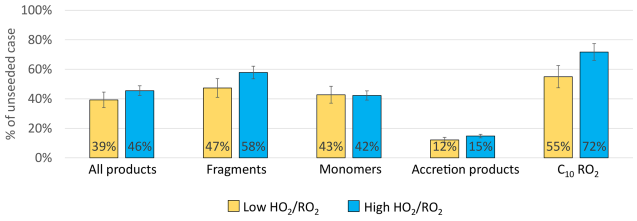

Figure 12. Overview of average, relative change in product classes signal between gas phase only and seeded system. Blue shows the high HO_2/RO_2 case, yellow the low HO_2/RO_2 case. (All are normalized to α-pinene OH turnover, *Exp2* experiment).

OH loss in the autoxidation chain of cyclohexene. Piletic and Kleindienst (2022) calculated fast reaction rate constants in the range of 1–30 s^{-1} for such intramolecular termination reactions to carbonyls for some $C_{10}H_{17}O_5$ in the α-pinene photooxidation, indicating that this pathway could also be significant for $C_{10}H_{15}O_x$. However, more investigation is necessary.

The overall contributions of the $C_{10}H_{14}O_z$, $C_{10}H_{16}O_z$ and $C_{10}H_{18}O_z$ families to the HOM-Mon class at high HO_2/RO_2 are shifted as shown in Fig. 11.

The contribution of $C_{10}H_{16}O_z$ is largest and remains similar in both cases, matching the already shown unchanged signal level in Fig. 6. This is the case because the $C_{10}H_{16}O_z$ family contains the alcohols from $C_{10}H_{15}O_x$+RO_2, carbonyls from $C_{10}H_{17}O_x$+RO_2 and hydroperoxides from $C_{10}H_{15}O_x$+HO_2 (see Fig. 1). A separation of the effects of enhanced HO_2 on this monomer family is difficult, as for the case where RO_2 termination dominates versus the case where HO_2 termination dominates, the loss of carbonyls and alcohols is partially compensated by the gain of hydroperoxides. A strong gain in hydroperoxides is clearly reflected in the strong increase in $C_{10}H_{18}O_z$ at high HO_2/RO_2.

Inspection of the $C_{10}H_{14}O_z$ and $C_{10}H_{18}O_z$ families shows that ∼ 13 % of the contribution by $C_{10}H_{14}O_z$ is lost (carbonyls, 33 % at low HO_2/RO_2) and is present instead as $C_{10}H_{18}O_z$ (hydroperoxides), giving $C_{10}H_{18}O_z$ a contribution of 38 % at high HO_2/RO_2.

4.4 Impact on condensable organic mass

In the previous sections, we demonstrated a shift of the product distribution by the shift from low to high HO_2/RO_2 conditions. We also showed that the changes could be rationalized by generic mechanistic considerations. We added $(NH_4)_2SO_4$ seed aerosol in two experiments to determine how the shift in the product distribution affects the condensable organic mass by determining the fraction which remained in the gas phase after seeding.

Figure 12 shows the fraction remaining for the sum of all products as well as for the individual product classes for the high and the low HO_2/RO_2 case. In both cases a significant reduction of products in the gas phase was observed with seed present. Overall, the sum of all products was reduced by around 60 %, with a slightly higher reduction in the low HO_2/RO_2 case. This can be attributed to the larger importance of HOM-Acc in the low HO_2/RO_2 case, as well as to a 10 % lower reduction of the HOM-Frag in the high HO_2/RO_2 case. In both cases a reduction of the HOM-RO_2 is observed, which indicates that the provided particle sink could have affected HOM formation chemistry but only moderately.

The total organic particulate mass was determined by AMS measurements and was 2.0 and 3.4 µg m^{-3} at high and low HO_2/RO_2 in the experiment (*Exp2*) displayed in Fig. 12. A reduction of condensed organic mass to 73 % ± 3 % at high HO_2/RO_2 (orange bar in Fig. 14) was observed on average. Since non-seeded and seeded experiments were conducted at otherwise the same conditions and we did not observe significant new particle formation, the gas-phase compositions can be directly compared. Therefore, we conclude that the shift in the product distribution led to a reduction of condensable material at the same α-pinene turnover with OH (and O_3).

We calculated the wall-loss-corrected SOA yields with the corrected SOA mass as shown in Eq. (4) and as described by Sarrafzadeh et al. (2016). To this end, we used $C_{10}H_{16}O_7$ as the lead HOM compound. In the two experiments with seed present (*Exp2.1* and *Exp3*) we had SOA yields of 7.3 % and 10.0 % at high HO_2/RO_2 and 10.0 % and 12.8 % at low HO_2/RO_2. The difference in the SOA yields between experiments can be explained by the slightly different OH concentrations and subsequent difference in contribution by photooxidation (see Table 1). Overall, our yields are in the lower range in comparison with the SOA yields reported by McFiggans et al. (2019) for the α-pinene photooxidation. However, our experiments were also performed at 5 °C higher temperature (20 °C) compared to 15 °C in McFiggans et al. (2019). The SOA yields show an absolute reduction of ∼ 3 % at high HO_2/RO_2 compared to low HO_2/RO_2 (relative a reduction of about 30 %). A reduction of the SOA yield of α-pinene by addition of CO was described before by McFiggans et al. (2019); however, there the α-pinene OH turnover was not held constant.

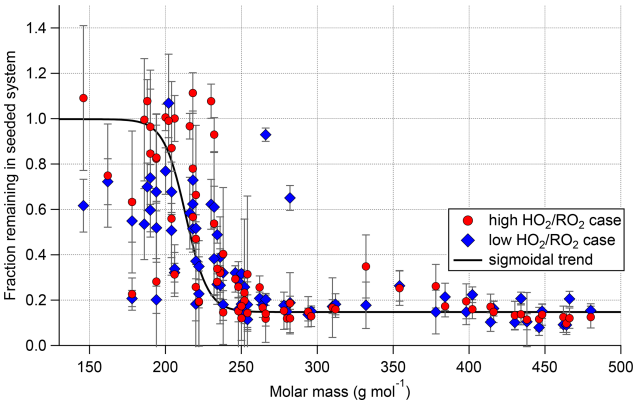

Figure 13. Gas-phase fraction remaining in the presence of seed (normalization of all data with α-pinene OH turnover) for the low (blue) and high (red) HO_2/RO_2 cases. Displayed points represent all closed-shell compounds that were detected with relative standard deviation <30 % in all four experiment phases. Error bars represent result of error propagation (see Supplement Sect. S9).

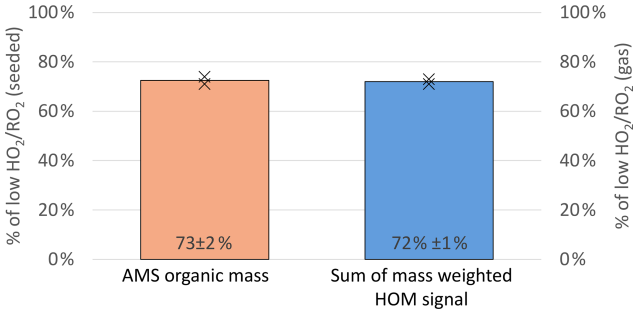

Figure 14. Overview of the average, relative change in organic mass observed in the AMS (left y axis, seeded experiments) and the mass-weighted HOM signal observed in the NO_3-CIMS (right y axis, unseeded experiments) between the low and high HO_2/RO_2 cases (both normalized to α-pinene OH turnover).

The change from the low to high HO_2/RO_2 regime favored termination reactions to protic termination groups, as we observed less carbonyl compounds and more hydroperoxides. This could, overall, shift the product distribution to products with lower vapor pressures and favor SOA formation, since protic groups can act as hydrogen bond donors as well as hydrogen bond acceptors (as exemplified by the comparison of ethanol (boiling point (b.p.) 78 °C) and ethane hydroperoxide (b.p. 93–97 °C) with acetaldehyde (b.p. 20 °C) (Richter et al., 1955)). However, the effect of the termination group should be small for HOMs as they likely contain multiple hydroperoxide groups (compare Pullinen et al., 2020). The reduction in HOM-Acc is expected to decrease the condensable mass, since the HOM-Acc scavenge non-HOM-RO_2 that would otherwise not partition into the particle phase.

Which of the measured compounds contribute significantly to the organic particle mass can be inferred by comparing their signal from the pure gas-phase, unseeded cases to their signal with seed in the system. Under the assumptions that for most HOM compounds re-evaporation to the gas phase is negligible and that the precursor chemistry is not substantially disturbed by seed addition, the fraction of signal remaining with seed in the system reflects to which degree the compound is condensing. Figure 13 shows the fraction remaining with seed in the system plotted against the molar mass of each individual compound. The plot includes all closed-shell products that were measured with a relative standard deviation of less than 30 % for all measurement phases and depicts the results for both the high and low HO_2/RO_2 cases.

Overall, in both cases we observed the same trend. Lighter compounds are not affected by the presence of seed particles, but with increasing molar mass the fraction remaining in the gas phase is reduced. A difference between the low and high HO_2/RO_2 cases can be observed in the low molar mass range: in the high HO_2/RO_2 case many fragmentation products show a higher gas-phase fraction remaining up to 1. (In some cases, values larger than 1 were observed but within the error limits. For the error estimation, see Supplement Sect. S9.) Fractions remaining larger than 1 beyond error could be an indication that such products have a particle-phase production source. Figure 13 also shows a critical semi-volatile to low-volatility organic compound molar mass region for molar masses between 175 and 250 g mol^{-1} where neither a fraction remaining of 1 nor complete condensation was observed. The position of this region on the molar mass scale depends on the provided organic mass concentration. The large variation of the fraction remaining in this small range of molar masses shows that the partitioning coefficients are dependent on the detailed structure of the compounds and not simply on their molar mass. The semi-volatile and low-volatility products represent mainly higher oxidized fragments and HOM-Mon with less than eight oxygens.

For compounds with a molar mass larger than 250 g mol^{-1}, a constant fraction remaining is reached in steady state, which is due to an ongoing production of the compounds. From the condensation behavior shown in Fig. 13, we conclude that the compounds heavier than 230 g mol^{-1} are expected to be of sufficiently low volatility to be mainly found in the particle phase for the organic mass present in the system and therefore contribute significantly to the SOA mass formation. Our finding agrees with the threshold used for low-volatility HOM products in Pullinen et al. (2020).

Therefore, the signal of all compounds with a molar mass heavier than 230 g mol^{-1} was weighted with their molar mass and summed (see Eq. 2). The ratio of this weighted signal sum at low and high HO_2/RO_2 is then a measure of expected SOA mass loss. The calculation leads to an expected reduction to 72 % (blue bar, Fig. 14). This simplified approach leads to a good agreement with the AMS measure-

ments and can thus explain the reduced particulate organic mass within the errors.

To test for closure between HOM lost and particulate organic mass measured, we approximated the upper limit of HOM concentration in the condensed phase. For this calculation, we used the calibration factor determined for sulfuric acid for our NO_3-MION-CIMS (7.0×10^9 molecules cm^{-3} $ncps^{-1}$, where ncps represents normalized counts per second) and the relationship between gas and particulate concentration of a compound in the SAPHIR-STAR chamber described in Eq. (3). Again, we considered all compounds with $M > 230\,g\,mol^{-1}$ in our calculation. The summed mass concentration lost from the gas phase was then compared to the SOA mass measured in the AMS. This comparison yields a good agreement within the uncertainties. The detailed calculation results can be found in the Supplement (Fig. S3). Overall, an agreement within 40 % is achieved for all measurement stages.

The comparisons presented above show that we understand the processes governing the SOA formation in our chamber and that the NO_3-CIMS measurements are well suited to observe the critical changes to understand the reduction in condensable organic material when shifting from low to high HO_2/RO_2.

5 Conclusions

In the presented series of experiments, we achieved a shift from a RO_2+RO_2-dominated chemistry to a more atmospherically relevant HO_2/RO_2 ratio under constant α-pinene OH turnover. It was shown that moving towards atmospheric HO_2/RO_2 ratio affected the SOA formation potential, with the observed organic mass being reduced at high HO_2/RO_2. This is in support of the potential bias towards high SOA yields in chamber studies at low HO_2/RO_2 as discussed by Schervish and Donahue (2021). Our results confirm that too low HO_2/RO_2 is one important parameter that can lead to an overestimated SOA yield in laboratory studies. In a broader picture, the results show how important it is to consider the different contributions to the HOM-RO_2 sink (e.g., HO_2, RO_2, NO) when designing experiments and transferring laboratory results to the real atmosphere.

The gas-phase observations showed that the SOA reduction at high HO_2/RO_2 was mainly due to a reduced HOM-Acc formation, which were formed by RO_2+RO_2 cross-reactions in the low HO_2/RO_2 case. This prevented contribution to SOA by less oxidized RO_2 compounds which were scavenged in the HOM-Acc at low HO_2/RO_2. Under atmospheric conditions, such cross-reactions are less important, and such (mixed) accretion products would contribute less to SOA.

The overall observed HOM products were reduced slightly, showing that under certain circumstances RO_2+HO_2 termination can impede the HOM formation, mainly by reducing the precursor RO_2 levels and less by impeding the autoxidation itself. The autoxidation chain (once initiated) runs to a similar oxidation level at both high and low HO_2/RO_2. The observed HOM-Mon products shift significantly between monomer families due to the different termination reactions. A decrease in carbonyl and alcohol formation from RO_2+RO_2 and an increase in hydroperoxide formation from RO_2+HO_2 were observed at high HO_2/RO_2.

Furthermore, a reduction in HOM-Frag products, especially with lower carbon numbers, and a reduction in the parity of the $C_{10}H_{15}O_x$ HOM-RO_2 show a reduction in alkoxy radical formation at high HO_2/RO_2. The moderate reduction in larger HOM-Frag products and pinonaldehyde, however, suggests that some alkoxy radical steps are still important. This raises the question of whether alkoxy radical formation can be facilitated by HO_2. In the atmosphere such effects are most often overcome whenever RO_2+NO is the major alkoxy radical source.

Overall, the observed changes in the gas phase could be well explained with the presented generic mechanistic understanding of HOM formation in the α-pinene system. The addition of seed particles demonstrated that the shift towards high HO_2/RO_2 reduced the condensable organic mass, stressing the importance of controlling higher-order reactions of peroxy radicals which lead to overemphasis on HOM-Acc product formation at low HO_2/RO_2 ratios.

Furthermore, the seed addition allowed us to determine which products were contributing to the SOA formation and show that their volatility is a function of molar mass and detailed molecular structure. This revealed a critical molar mass region in which compounds have significant fractions in gas and particulate phases. Based on absorptive partitioning theory, the volatilities at which this critical region is found should depend on the organic mass present in the system.

Valuable insight about the condensed phase can be gained from HOM gas-phase measurements. We inferred conclusions about the particulate phase from the gas-phase measurements and compared them to the direct particle-phase observations, finding good agreements between our expectations and the measurements.

Data availability. Information about all steady-state conditions utilized and the data necessary to reproduce the figures in this study are available at https://doi.org/10.26165/JUELICH-DATA/R8ITFF (Baker et al., 2024).

Supplement. The supplement related to this article is available online at: https://doi.org/10.5194/acp-24-4789-2024-supplement.

Author contributions. TFM, MH and GM conceptualized the study, and TFM, YB, SK and SRZ designed the experiments and developed the analysis methodology. The experiments were performed by YB, SK, VG and SRZ. Instrument deployment and/or data analysis were performed by YB, SK, HW, RW, JX, AZ, QH, TZ and VG. YB did model calculations of the experiments. AV, SPO, TJB, MG and MH provided counsel on experiment design and data interpretation. The compiled data set was interpreted by YB and TFM, and the results were discussed by all co-authors. YB visualized the data, and YB and TFM prepared the manuscript. All co-authors reviewed the manuscript.

Competing interests. The contact author has declared that none of the authors has any competing interests.

Disclaimer. Publisher's note: Copernicus Publications remains neutral with regard to jurisdictional claims made in the text, published maps, institutional affiliations, or any other geographical representation in this paper. While Copernicus Publications makes every effort to include appropriate place names, the final responsibility lies with the authors.

Financial support. This research has received funding from the European Union's Horizon 2020 research and innovation programme under the FORCeS project under grant agreement no. 821205, the German Federal Ministry of Education and Research (BMBF) under the FONA Strategy "Research for Sustainability" as part of the implementation of ACTRIS-D under the funding code 01LK200010, Vetenskapsrådet (VR, grant agreement no. 2018-04430), Svenska Forskningsrådet Formas (grant agreement no. 2019-586) and the UK Natural Environment Research Council (NERC) under grant agreement no. NE/V012665/1.

The article processing charges for this open-access publication were covered by the Forschungszentrum Jülich.

Review statement. This paper was edited by Sergey A. Nizkorodov and reviewed by two anonymous referees.

References

Albrecht, S. R., Novelli, A., Hofzumahaus, A., Kang, S., Baker, Y., Mentel, T., Wahner, A., and Fuchs, H.: Measurements of hydroperoxy radicals (HO_2) at atmospheric concentrations using bromide chemical ionisation mass spectrometry, Atmos. Meas. Tech., 12, 891–902, https://doi.org/10.5194/amt-12-891-2019, 2019.

Atkinson, R. and Arey, J.: Atmospheric degradation of volatile organic compounds, Chem. Rev., 103, 4605–4638, https://doi.org/10.1021/cr0206420, 2003.

Baker, Y., Kang, S., Wang, H., Wu, R., Xu, J., Zanders, A., He, Q., Hohaus, T., Ziehm, T., Geretti, V., Bannan, T. J., O'Meara, S. P., Voliotis, A., Hallquist, M., McFiggans, G., Zorn, S. R., Wahner, A., Mentel, T.: "Supplementary data for "Impact of HO_2/RO_2 ratio on highly oxygenated α-pinene photooxidation products and secondary organic aerosol formation potential", Jülich DATA [data set], V1, https://doi.org/10.26165/JUELICH-DATA/R8ITFF, 2024.

Berndt, T.: Peroxy Radical Processes and Product Formation in the OH Radical-Initiated Oxidation of α-Pinene for Near-Atmospheric Conditions, J. Phys. Chem. A, 125, 9151–9160, https://doi.org/10.1021/acs.jpca.1c05576, 2021.

Berndt, T., Richters, S., Jokinen, T., Hyttinen, N., Kurtén, T., Otkjaer, R. V., Kjaergaard, H. G., Stratmann, F., Herrmann, H., Sipila, M., Kulmala, M., and Ehn, M.: Hydroxyl radical-induced formation of highly oxidized organic compounds, Nat. Commun., 7, 13677, https://doi.org/10.1038/ncomms13677, 2016.

Berndt, T., Mentler, B., Scholz, W., Fischer, L., Herrmann, H., Kulmala, M., and Hansel, A.: Accretion product formation from ozonolysis and OH radical reaction of α-pinene: mechanistic insight and the influence of isoprene and ethylene, Environ. Sci. Technol., 52, 11069–11077, https://doi.org/10.1021/acs.est.8b02210, 2018.

Bianchi, F., Garmash, O., He, X., Yan, C., Iyer, S., Rosendahl, I., Xu, Z., Rissanen, M. P., Riva, M., Taipale, R., Sarnela, N., Petäjä, T., Worsnop, D. R., Kulmala, M., Ehn, M., and Junninen, H.: The role of highly oxygenated molecules (HOMs) in determining the composition of ambient ions in the boreal forest, Atmos. Chem. Phys., 17, 13819–13831, https://doi.org/10.5194/acp-17-13819-2017, 2017.

Bianchi, F., Kurtén, T., Riva, M., Mohr, C., Rissanen, M. P., Roldin, P., Berndt, T., Crounse, J. D., Wennberg, P. O., Mentel, T. F., Wildt, J., Junninen, H., Jokinen, T., Kulmala, M., Worsnop, D. R., Thornton, J. A., Donahue, N., Kjaergaard, H. G., and Ehn, M.: Highly Oxygenated Organic Molecules (HOM) from Gas-Phase Autoxidation Involving Peroxy Radicals: A Key Contributor to Atmospheric Aerosol, Chem. Rev., 119, 3472–3509, https://doi.org/10.1021/acs.chemrev.8b00395, 2019.

Cox, R. A., Ammann, M., Crowley, J. N., Herrmann, H., Jenkin, M. E., McNeill, V. F., Mellouki, A., Troe, J., and Wallington, T. J.: Evaluated kinetic and photochemical data for atmospheric chemistry: Volume VII – Criegee intermediates, Atmos. Chem. Phys., 20, 13497–13519, https://doi.org/10.5194/acp-20-13497-2020, 2020.

Crounse, J. D., Nielsen, L. B., Jørgensen, S., Kjaergaard, H. G., and Wennberg, P. O.: Autoxidation of organic compounds in the atmosphere, J. Phys. Chem. Lett., 4, 3513–3520, https://doi.org/10.1021/jz4019207, 2013.

Docherty, K. S. and Ziemann, P. J.: Effects of stabilized criegee intermediate and OH radical scavengers on aerosol formation from reactions of β-pinene with O_3, Aerosol Sci. Tech., 37, 877–891, https://doi.org/10.1080/02786820300930, 2003.

Eddingsaas, N. C., Loza, C. L., Yee, L. D., Seinfeld, J. H., and Wennberg, P. O.: α-pinene photooxidation under controlled chemical conditions – Part 1: Gas-phase composition in low- and high-NO_x environments, Atmos. Chem. Phys., 12, 6489–6504, https://doi.org/10.5194/acp-12-6489-2012, 2012.

Ehn, M., Thornton, J. A., Kleist, E., Sipila, M., Junninen, H., Pullinen, I., Springer, M., Rubach, F., Tillmann, R., Lee, B., Lopez-Hilfiker, F., Andres, S., Acir, I. H., Rissanen, M., Jokinen, T., Schobesberger, S., Kangasluoma, J., Kontkanen, J., Nieminen, T., Kurtén, T., Nielsen, L. B., Jorgensen, S., Kjaergaard, H. G., Canagaratna, M., Maso, M. D., Berndt, T., Petaja,

T., Wahner, A., Kerminen, V. M., Kulmala, M., Worsnop, D. R., Wildt, J., and Mentel, T. F.: A large source of low-volatility secondary organic aerosol, Nature, 506, 476–479, https://doi.org/10.1038/nature13032, 2014.

Eisele, F. and Tanner, D.: Measurement of the gas phase concentration of H_2SO_4 and methane sulfonic acid and estimates of H_2SO_4 production and loss in the atmosphere, J. Geophys. Res.-Atmos., 98, 9001–9010, https://doi.org/10.1029/93JD00031, 1993.

Fantechi, G., Vereecken, L., and Peeters, J.: The OH-initiated atmospheric oxidation of pinonaldehyde: Detailed theoretical study and mechanism construction, Phys. Chem. Chem. Phys., 4, 5795–5805, https://doi.org/10.1039/B205901K 2002.

Guo, Y., Shen, H., Pullinen, I., Luo, H., Kang, S., Vereecken, L., Fuchs, H., Hallquist, M., Acir, I.-H., Tillmann, R., Rohrer, F., Wildt, J., Kiendler-Scharr, A., Wahner, A., Zhao, D., and Mentel, T. F.: Identification of highly oxygenated organic molecules and their role in aerosol formation in the reaction of limonene with nitrate radical, Atmos. Chem. Phys., 22, 11323–11346, https://doi.org/10.5194/acp-22-11323-2022, 2022.

Hallquist, M., Wenger, J. C., Baltensperger, U., Rudich, Y., Simpson, D., Claeys, M., Dommen, J., Donahue, N. M., George, C., Goldstein, A. H., Hamilton, J. F., Herrmann, H., Hoffmann, T., Iinuma, Y., Jang, M., Jenkin, M. E., Jimenez, J. L., Kiendler-Scharr, A., Maenhaut, W., McFiggans, G., Mentel, Th. F., Monod, A., Prévôt, A. S. H., Seinfeld, J. H., Surratt, J. D., Szmigielski, R., and Wildt, J.: The formation, properties and impact of secondary organic aerosol: current and emerging issues, Atmos. Chem. Phys., 9, 5155–5236, https://doi.org/10.5194/acp-9-5155-2009, 2009.

Hantschke, L. L.: Oxidation of monoterpenes studied in atmospheric simulation chambers, Forschungszentrum Jülich GmbH, Zentralbibliothek, Verlag, ISBN 978-3-95806-653-3, 2022.

Hasson, A. S., Kuwata, K. T., Arroyo, M. C., and Petersen, E. B.: Theoretical studies of the reaction of hydroperoxy radicals (HO_2) with ethyl peroxy ($CH_3CH_2O_2$), acetyl peroxy ($CH_3C(O)O_2$), and acetonyl peroxy ($CH_3C(O)CH_2O_2$) radicals, J. Photochem. Photobiol. A, 176, 218–230, https://doi.org/10.1016/j.jphotochem.2005.08.012, 2005.

Henry, K. M., Lohaus, T., and Donahue, N. M.: Organic aerosol yields from α-pinene oxidation: bridging the gap between first-generation yields and aging chemistry, Environ. Sci. Technol., 46, 12347–12354, https://doi.org/10.1021/es302060y, 2012.

Hidy, G.: Atmospheric chemistry in a box or a bag, Atmos., 10, 401, https://doi.org/10.3390/atmos10070401, 2019.

Hyttinen, N., Otkjær, R. V., Iyer, S., Kjaergaard, H. G., Rissanen, M. P., Wennberg, P. O., and Kurtén, T.: Computational comparison of different reagent ions in the chemical ionization of oxidized multifunctional compounds, J. Phys. Chem. A, 122, 269–279, https://doi.org/10.1021/acs.jpca.7b10015, 2018.

Iyer, S., Reiman, H., Møller, K. H., Rissanen, M. P., Kjaergaard, H. G., and Kurtén, T.: Computational investigation of $RO_2 + HO_2$ and $RO_2 + RO_2$ reactions of monoterpene derived first-generation peroxy radicals leading to radical recycling, J. Phys. Chem. A, 122, 9542–9552, https://doi.org/10.1021/acs.jpca.8b09241, 2018.

Iyer, S., Rissanen, M. P., Valiev, R., Barua, S., Krechmer, J. E., Thornton, J., Ehn, M., and Kurtén, T.: Molecular mechanism for rapid autoxidation in α-pinene ozonolysis, Nat. Commun., 12, 878, https://doi.org/10.1038/s41467-021-21172-w, 2021.

Jenkin, M. E., Saunders, S. M., and Pilling, M. J.: The tropospheric degradation of volatile organic compounds: a protocol for mechanism development, Atmos. Environ., 31, 81–104, https://doi.org/10.1016/S1352-2310(96)00105-7, 1997.

Jenkin, M. E., Valorso, R., Aumont, B., and Rickard, A. R.: Estimation of rate coefficients and branching ratios for reactions of organic peroxy radicals for use in automated mechanism construction, Atmos. Chem. Phys., 19, 7691–7717, https://doi.org/10.5194/acp-19-7691-2019, 2019.

Johnson, D. and Marston, G.: The gas-phase ozonolysis of unsaturated volatile organic compounds in the troposphere, Chem. Soc. Rev., 37, 699–716, https://doi.org/10.1039/B704260B 2008.

Junninen, H., Ehn, M., Petäjä, T., Luosujärvi, L., Kotiaho, T., Kostiainen, R., Rohner, U., Gonin, M., Fuhrer, K., Kulmala, M., and Worsnop, D. R.: A high-resolution mass spectrometer to measure atmospheric ion composition, Atmos. Meas. Tech., 3, 1039–1053, https://doi.org/10.5194/amt-3-1039-2010, 2010.

Kang, S.: Formation of highly oxygenated organic molecules from α-pinene photochemistry, Forschungszentrum Jülich GmbH, 156 pp., https://doi.org/10.25926/rd20-nb07, 2021.

Keywood, M., Kroll, J., Varutbangkul, V., Bahreini, R., Flagan, R., and Seinfeld, J.: Secondary organic aerosol formation from cyclohexene ozonolysis: Effect of OH scavenger and the role of radical chemistry, Environ. Sci. Technol., 38, 3343–3350, https://doi.org/10.1021/es049725j, 2004.

Khan, M., Cooke, M., Utembe, S., Archibald, A., Derwent, R., Jenkin, M. E., Morris, W., South, N., Hansen, J., Francisco, J., Percival, C. J., and Shallcross, D. E.: Global analysis of peroxy radicals and peroxy radical-water complexation using the STOCHEM-CRI global chemistry and transport model, Atmos. Environ., 106, 278–287, https://doi.org/10.1016/j.atmosenv.2015.02.020, 2015.

Kiendler-Scharr, A., Wildt, J., Maso, M. D., Hohaus, T., Kleist, E., Mentel, T. F., Tillmann, R., Uerlings, R., Schurr, U., and Wahner, A.: New particle formation in forests inhibited by isoprene emissions, Nature, 461, 381–384, https://doi.org/10.1038/nature08292, 2009.

McFiggans, G., Mentel, T. F., Wildt, J., Pullinen, I., Kang, S., Kleist, E., Schmitt, S., Springer, M., Tillmann, R., Wu, C., Zhao, D., Hallquist, M., Faxon, C., Le Breton, M., Hallquist, A. M., Simpson, D., Bergstrom, R., Jenkin, M. E., Ehn, M., Thornton, J. A., Alfarra, M. R., Bannan, T. J., Percival, C. J., Priestley, M., Topping, D., and Kiendler-Scharr, A.: Secondary organic aerosol reduced by mixture of atmospheric vapours, Nature, 565, 587–593, https://doi.org/10.1038/s41586-018-0871-y, 2019.

Mentel, T. F., Springer, M., Ehn, M., Kleist, E., Pullinen, I., Kurtén, T., Rissanen, M., Wahner, A., and Wildt, J.: Formation of highly oxidized multifunctional compounds: autoxidation of peroxy radicals formed in the ozonolysis of alkenes – deduced from structure–product relationships, Atmos. Chem. Phys., 15, 6745–6765, https://doi.org/10.5194/acp-15-6745-2015, 2015.

Mentel, Th. F., Wildt, J., Kiendler-Scharr, A., Kleist, E., Tillmann, R., Dal Maso, M., Fisseha, R., Hohaus, Th., Spahn, H., Uerlings, R., Wegener, R., Griffiths, P. T., Dinar, E., Rudich, Y., and Wahner, A.: Photochemical production of aerosols from real plant emissions, Atmos. Chem. Phys., 9, 4387–4406, https://doi.org/10.5194/acp-9-4387-2009, 2009.

Mohr, C., Thornton, J. A., Heitto, A., Lopez-Hilfiker, F. D., Lutz, A., Riipinen, I., Hong, J., Donahue, N. M., Hallquist, M., Petaja, T., Kulmala, M., and Yli-Juuti, T.: Molecular identification of organic vapors driving atmospheric nanoparticle growth, Nat. Commun., 10, 4442, https://doi.org/10.1038/s41467-019-12473-2, 2019.

Otkjaer, R. V., Jakobsen, H. H., Tram, C. M., and Kjaergaard, H. G.: Calculated Hydrogen Shift Rate Constants in Substituted Alkyl Peroxy Radicals, J. Phys. Chem. A, 122, 8665–8673, https://doi.org/10.1021/acs.jpca.8b06223, 2018.

Piletic, I. R. and Kleindienst, T. E.: Rates and yields of unimolecular reactions producing highly oxidized peroxy radicals in the OH-induced autoxidation of α-pinene, β-pinene, and limonene, J. Phys. Chem. A, 126, 88–100, https://doi.org/10.1021/acs.jpca.1c07961, 2022.

Pullinen, I., Schmitt, S., Kang, S., Sarrafzadeh, M., Schlag, P., Andres, S., Kleist, E., Mentel, T. F., Rohrer, F., Springer, M., Tillmann, R., Wildt, J., Wu, C., Zhao, D., Wahner, A., and Kiendler-Scharr, A.: Impact of NO_x on secondary organic aerosol (SOA) formation from α-pinene and β-pinene photooxidation: the role of highly oxygenated organic nitrates, Atmos. Chem. Phys., 20, 10125–10147, https://doi.org/10.5194/acp-20-10125-2020, 2020.

Richter, F., Ostertag, R., Ammerlahn, G., Behrle, E., Baumann, M., and Kobel, M. (Eds.): Beilstein's handbook of organic chemistry. Third supplement, covering the literature from 1930–1949, Beilstein's handbook of organic chemistry, Springer, Berlin, 1955.

Rissanen, M. P., Mikkilä, J., Iyer, S., and Hakala, J.: Multi-scheme chemical ionization inlet (MION) for fast switching of reagent ion chemistry in atmospheric pressure chemical ionization mass spectrometry (CIMS) applications, Atmos. Meas. Tech., 12, 6635–6646, https://doi.org/10.5194/amt-12-6635-2019, 2019.

Rissanen, M. P., Kurtén, T., Sipila, M., Thornton, J. A., Kangasluoma, J., Sarnela, N., Junninen, H., Jorgensen, S., Schallhart, S., Kajos, M. K., Taipale, R., Springer, M., Mentel, T. F., Ruuskanen, T., Petaja, T., Worsnop, D. R., Kjaergaard, H. G., and Ehn, M.: The formation of highly oxidized multifunctional products in the ozonolysis of cyclohexene, J. Am. Chem. Soc., 136, 15596–15606, https://doi.org/10.1021/ja507146s, 2014.

Roldin, P., Ehn, M., Kurtén, T., Olenius, T., Rissanen, M. P., Sarnela, N., Elm, J., Rantala, P., Hao, L., Hyttinen, N., Heikkinen, L., Worsnop, D. R., Pichelstorfer, L., Xavier, C., Clusius, P., Öström, E., Petäjä, T., Kulmala, M., Vehkamäki, H., Virtanen, A., Riipinen, I., and Boy, M.: The role of highly oxygenated organic molecules in the Boreal aerosol-cloud-climate system, Nat. Commun., 10, 4370, https://doi.org/10.1038/s41467-019-12338-8, 2019.

Sanchez, J., Tanner, D. J., Chen, D., Huey, L. G., and Ng, N. L.: A new technique for the direct detection of HO_2 radicals using bromide chemical ionization mass spectrometry (Br-CIMS): initial characterization, Atmos. Meas. Tech., 9, 3851–3861, https://doi.org/10.5194/amt-9-3851-2016, 2016.

Sarrafzadeh, M., Wildt, J., Pullinen, I., Springer, M., Kleist, E., Tillmann, R., Schmitt, S. H., Wu, C., Mentel, T. F., Zhao, D., Hastie, D. R., and Kiendler-Scharr, A.: Impact of NO_x and OH on secondary organic aerosol formation from β-pinene photooxidation, Atmos. Chem. Phys., 16, 11237–11248, https://doi.org/10.5194/acp-16-11237-2016, 2016.

Saunders, S. M., Jenkin, M. E., Derwent, R. G., and Pilling, M. J.: Protocol for the development of the Master Chemical Mechanism, MCM v3 (Part A): tropospheric degradation of non-aromatic volatile organic compounds, Atmos. Chem. Phys., 3, 161–180, https://doi.org/10.5194/acp-3-161-2003, 2003.

Schervish, M. and Donahue, N. M.: Peroxy radical kinetics and new particle formation, Environ. Sci. Atmos., 1, 79–92, https://doi.org/10.1039/d0ea00017e, 2021.

Shen, H., Zhao, D., Pullinen, I., Kang, S., Vereecken, L., Fuchs, H., Acir, I. H., Tillmann, R., Rohrer, F., Wildt, J., Kiendler-Scharr, A., Wahner, A., and Mentel, T. F.: Highly Oxygenated Organic Nitrates Formed from NO(3) Radical-Initiated Oxidation of β-Pinene, Environ. Sci. Technol., 55, 15658–15671, https://doi.org/10.1021/acs.est.1c03978, 2021.

Shen, H., Vereecken, L., Kang, S., Pullinen, I., Fuchs, H., Zhao, D., and Mentel, T. F.: Unexpected significance of a minor reaction pathway in daytime formation of biogenic highly oxygenated organic compounds, Sci. Adv., 8, eabp8702, https://doi.org/10.1126/sciadv.abp8702, 2022.

Shilling, J. E., Chen, Q., King, S. M., Rosenoern, T., Kroll, J. H., Worsnop, D. R., DeCarlo, P. F., Aiken, A. C., Sueper, D., Jimenez, J. L., and Martin, S. T.: Loading-dependent elemental composition of α-pinene SOA particles, Atmos. Chem. Phys., 9, 771–782, https://doi.org/10.5194/acp-9-771-2009, 2009.

Vereecken, L. and Nozière, B.: H migration in peroxy radicals under atmospheric conditions, Atmos. Chem. Phys., 20, 7429–7458, https://doi.org/10.5194/acp-20-7429-2020, 2020.

Vereecken, L., Müller, J.-F., and Peeters, J.: Low-volatility poly-oxygenates in the OH-initiated atmospheric oxidation of α-pinene: impact of non-traditional peroxyl radical chemistry, Phys. Chem. Chem. Phys., 9, 5241–5248, https://doi.org/10.1039/b708023a, 2007.

Wildt, J., Mentel, T. F., Kiendler-Scharr, A., Hoffmann, T., Andres, S., Ehn, M., Kleist, E., Müsgen, P., Rohrer, F., Rudich, Y., Springer, M., Tillmann, R., and Wahner, A.: Suppression of new particle formation from monoterpene oxidation by NO_x, Atmos. Chem. Phys., 14, 2789–2804, https://doi.org/10.5194/acp-14-2789-2014, 2014.

Xu, L., Møller, K. H., Crounse, J. D., Otkjær, R. V., Kjaergaard, H. G., and Wennberg, P. O.: Unimolecular reactions of peroxy radicals formed in the oxidation of α-pinene and β-pinene by hydroxyl radicals, J. Phys. Chem. A, 123, 1661–1674, https://doi.org/10.1021/acs.jpca.8b11726, 2019.